

# NAVAL POSTGRADUATE SCHOOL MONTEREY, CALIFORNIA



## THESIS

### WAVE/CURRENT INDUCED FORCES ON CIRCULAR CYLINDERS

by

Marc S. de Angelis

December, 1995

Thesis Advisor:

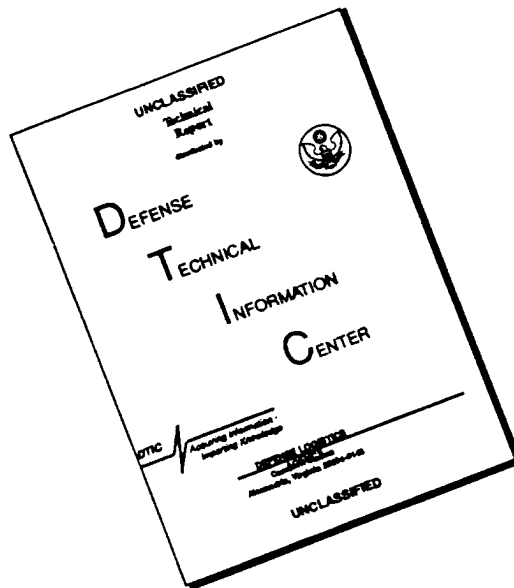
T. Sarpkaya

Approved for public release; distribution is unlimited.

19960411 114

DTIC QUALITY INSPECTED 1

# DISCLAIMER NOTICE



THIS DOCUMENT IS BEST QUALITY AVAILABLE. THE COPY FURNISHED TO DTIC CONTAINED A SIGNIFICANT NUMBER OF PAGES WHICH DO NOT REPRODUCE LEGIBLY.

REPORT DOCUMENTATION PAGE			Form Approved OMB No. 0704-0188	
Public reporting burden for this collection of information is estimated to average 1 hour per response, including the time for reviewing instruction, searching existing data sources, gathering and maintaining the data needed, and completing and reviewing the collection of information. Send comments regarding this burden estimate or any other aspect of this collection of information, including suggestions for reducing this burden, to Washington Headquarters Services, Directorate for Information Operations and Reports, 1215 Jefferson Davis Highway, Suite 1204, Arlington, VA 22202-4302, and to the Office of Management and Budget, Paperwork Reduction Project (0704-0188) Washington DC 20503.				
1. AGENCY USE ONLY (Leave blank)		2. REPORT DATE December 1995		3. REPORT TYPE AND DATES COVERED Master's Thesis
4. TITLE AND SUBTITLE WAVE/CURRENT INDUCED FORCES ON CIRCULAR CYLINDERS			5. FUNDING NUMBERS	
6. AUTHOR(S) de Angelis, Marc, S				
7. PERFORMING ORGANIZATION NAME(S) AND ADDRESS(ES) Naval Postgraduate School Monterey CA 93943-5000			8. PERFORMING ORGANIZATION REPORT NUMBER	
9. SPONSORING/MONITORING AGENCY NAME(S) AND ADDRESS(ES)			10. SPONSORING/MONITORING AGENCY REPORT NUMBER	
11. SUPPLEMENTARY NOTES The views expressed in this thesis are those of the author and do not reflect the official policy or position of the Department of Defense or the U.S. Government.				
12a. DISTRIBUTION/AVAILABILITY STATEMENT Approved for public release; distribution is unlimited.			12b. DISTRIBUTION CODE	
13. ABSTRACT (maximum 200 words) The numerical simulations of oscillating plus mean flow past a circular cylinder have been carried out in detail through the use of a commercially available software produced by CFDRC, running on a Silicon Graphics Inc. Indigo 2 Extreme computer. The Reynolds number, Keulegan-Carpenter number, and relative current velocity were systematically varied. Sensitivity analysis was performed to delineate the effects of time step, turbulence model and numerical schemes. The results have been compared to those obtained experimentally and to those predicted by the Morison Equation. In many cases the predicted force coefficients have shown good agreement with those obtained experimentally.				
14. SUBJECT TERMS CFD, Oscillating Flows, Cylinders			15. NUMBER OF PAGES 78	
			16. PRICE CODE	
17. SECURITY CLASSIFICATION OF REPORT Unclassified	18. SECURITY CLASSIFICATION OF THIS PAGE Unclassified	19. SECURITY CLASSIFICATION OF ABSTRACT Unclassified	20. LIMITATION OF ABSTRACT UL	

NSN 7540-01-280-5500

Standard Form 298 (Rev. 2-89)  
Prescribed by ANSI Std. Z39-18 298-102



Approved for public release; distribution is unlimited.

**WAVE/CURRENT INDUCED FORCES  
ON CIRCULAR CYLINDERS**

Marc S. de Angelis  
Lieutenant Commander, United States Navy  
B.S., Villanova University, 1981

Submitted in partial fulfillment  
of the requirements for the degree of

**MASTER OF SCIENCE IN MECHANICAL ENGINEERING**

from the

**NAVAL POSTGRADUATE SCHOOL**

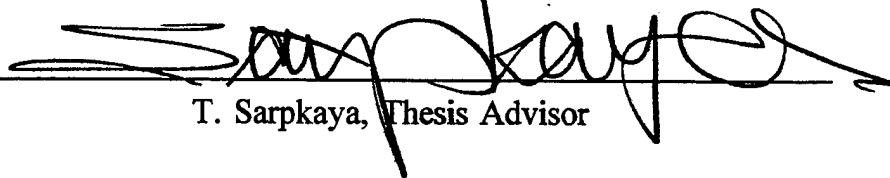
**December 1995**

Author:



Marc S. de Angelis

Approved by:



T. Sarpkaya, Thesis Advisor



Matthew Kelleher, Chairman  
Department of Mechanical Engineering



## ABSTRACT

The numerical simulations of oscillating plus mean flow past a circular cylinder have been carried out in detail through the use of a commercially available software produced by CFDRC, running on a Silicon Graphics Inc. Indigo 2 Extreme computer. The Reynolds number, Keulegan-Carpenter number, and relative current velocity were systematically varied. Sensitivity analysis was performed to delineate the effects of time step, turbulence model and numerical schemes. The results have been compared to those obtained experimentally and to those predicted by the Morison Equation. In many cases the predicted force coefficients have shown good agreement with those obtained experimentally.



## TABLE OF CONTENTS

I. INTRODUCTION .....	1
II. BACKGROUND STUDIES .....	3
III. NUMERICAL REPRESENTATION .....	7
A. COMPUTATIONAL METHOD .....	7
B. GRID GENERATION .....	9
C. BOUNDARY CONDITIONS .....	10
D. FLOW CONTROL .....	11
E. DATA REDUCTION AND CALCULATION OF FORCE COEFFICIENTS .....	12
F. INPUT OPTIONS .....	13
IV. DISCUSSION OF RESULTS .....	17
A. INTRODUCTION .....	17
B. GRID AND INPUT PARAMETERS .....	17
C. IN-LINE AND TRANSVERSE FORCE COEFFICIENTS .....	19
D. FLOW VISUALIZATION .....	22
E. NUMERICAL RESULTS .....	22

F. SENSITIVITY ANALYSIS .....	23
V. CONCLUSIONS .....	29
APPENDIX A. FIGURES .....	31
APPENDIX B. RECOMMENDED VALUES FOR THE CURRENT VELOCITY- PRESSURE DIFFERENTIAL CORRELATION COEFFICIENT .....	49
APPENDIX C. SAMPLE IN-FILE .....	51
LIST OF REFERENCES .....	57
INITIAL DISTRIBUTION LIST .....	59

## LIST OF FIGURES

1.	Computational Grid .....	31
2a.	In-line force coefficient versus time. $K=8.6$ ; $\beta=1772$ ; $V_k=2.05$ . (k- $\epsilon$ turbulence model used) .....	32
2b.	Transverse force coefficient versus time. $K=8.6$ ; $\beta=1772$ ; $V_k=2.05$ . (k- $\epsilon$ turbulence model used) .....	32
2c.	In-line force coefficient versus time. $K=8.6$ ; $\beta=1772$ ; $V_k=2.05$ . (Low Re turbulence model used) .....	33
2d.	Transverse force coefficient versus time. $K=8.6$ ; $\beta=1772$ ; $V_k=2.05$ . (Low Re turbulence model used) .....	33
3.	In-line force coefficient versus time. $K=15$ ; $\beta=1772$ ; $V_k=2.05$ .....	34
4.	In-line force coefficient versus time. $K=36.5$ ; $\beta=1772$ ; $V_k=2.05$ .....	34
5a.	In-line force coefficient versus time. $K=8.78$ ; $\beta=1772$ ; $V_k=4$ .....	35
5b.	Transverse force coefficient versus time. $K=8.78$ ; $\beta=1772$ ; $V_k=4$ .....	35
6a.	In-line force coefficient versus time. $K=12.19$ ; $\beta=1772$ ; $V_k=4$ . (RNG turbulence model used) .....	36
6b.	Transverse force coefficient versus time. $K=12.19$ ; $\beta=1772$ ; $V_k=4$ . (RNG turbulence model used) .....	36
6c.	In-line force coefficient versus time. $K=12.19$ ; $\beta=1772$ ; $V_k=4$ . (Low Re turbulence model used) .....	37
6d.	Transverse force coefficient versus time. $K=12.19$ ; $\beta=1772$ ; $V_k=4$ . (Low Re turbulence model used) .....	37
7.	In-line force coefficient versus time. $K=26.07$ ; $\beta=1772$ ; $V_k=4$ .....	38
8.	In-line force coefficient versus time. $K=10.3$ ; $\beta=1772$ ; $V_k=4$ .....	38
9a.	In-line force coefficient versus time. $K=36.5$ ; $\beta=1772$ ; $V_k=6.05$ .....	39

9b.	Transverse force coefficient versus time. $K=36.5$ ; $\beta=1772$ ; $V_k=6.05$ .....	39
9c.	In-line force coefficient versus time. $K=36.5$ ; $\beta=1772$ ; $V_k=0$ .....	40
9d.	Transverse force coefficient versus time. $K=36.5$ ; $\beta=1772$ ; $V_k=0$ .....	40
10.	In-line force coefficient versus time. $K=10.5$ ; $\beta=2487$ ; $V_k=5.01$ .....	41
11.	In-line force coefficient versus time. $K=17.2$ ; $\beta=2487$ ; $V_k=5.01$ .....	41
12.	In-line force coefficient versus time. $K=46$ ; $\beta=2487$ ; $V_k=5.01$ .....	42
13.	In-line force coefficient versus time. $K=5.1$ ; $\beta=4122$ ; $V_k=2.07$ .....	42
14a.	In-line force coefficient versus time. $K=15$ ; $\beta=4122$ ; $V_k=2.07$ .....	43
14b.	Transverse force coefficient versus time. $K=15$ ; $\beta=4122$ ; $V_k=2.07$ .....	43
15a.	In-line force coefficient versus time. $K=24$ ; $\beta=4122$ ; $V_k=2.07$ .....	44
15b.	Transverse force coefficient versus time. $K=24$ ; $\beta=4122$ ; $V_k=2.07$ .....	44
16a.	Evolution of vorticity. $K=8.78$ , $\beta=1772$ ; $V_r=0.43$ , $u(t)/U_m=0.99$ .....	45
16b.	Evolution of vorticity. $K=8.78$ , $\beta=1772$ ; $V_r=0.43$ , $u(t)/U_m=0.5$ .....	45
16c.	Evolution of vorticity. $K=8.78$ , $\beta=1772$ ; $V_r=0.43$ , $u(t)/U_m=-0.02$ .....	45
16d.	Evolution of vorticity. $K=8.78$ , $\beta=1772$ ; $V_r=0.43$ , $u(t)/U_m=-0.42$ .....	45
16e.	Evolution of vorticity. $K=8.78$ , $\beta=1772$ ; $V_r=0.43$ , $u(t)/U_m=-0.58$ .....	45
16f.	Evolution of vorticity. $K=8.78$ , $\beta=1772$ ; $V_r=0.43$ , $u(t)/U_m=-0.46$ .....	45
17a.	Streamlines. $K=8.78$ , $\beta=1772$ ; $V_r=0.43$ , $u(t)/U_m=0.99$ .....	46
17b.	Streamlines. $K=8.78$ , $\beta=1772$ ; $V_r=0.43$ , $u(t)/U_m=0.5$ .....	46
17c.	Streamlines. $K=8.78$ , $\beta=1772$ ; $V_r=0.43$ , $u(t)/U_m=-0.02$ .....	46
17d.	Streamlines. $K=8.78$ , $\beta=1772$ ; $V_r=0.43$ , $u(t)/U_m=-0.42$ .....	46

17e.	Streamlines. $K=8.78$ , $\beta=1772$ ; $V_r=0.43$ , $u(t)/U_m = -0.58$ .....	46
17f.	Streamlines. $K=8.78$ , $\beta=1772$ ; $V_r=0.43$ , $u(t)/U_m = -0.46$ .....	46
18a.	Evolution of vorticity. $K=10.5$ , $\beta=2487$ ; $V_r=0.47$ , $u(t)/U_m = 0.11$ .....	47
18b.	Evolution of vorticity. $K=10.5$ , $\beta=2487$ ; $V_r=0.47$ , $u(t)/U_m = 0.98$ .....	47
18c.	Evolution of vorticity. $K=10.5$ , $\beta=2487$ ; $V_r=0.47$ , $u(t)/U_m = 1.46$ .....	47
18d.	Evolution of vorticity. $K=10.5$ , $\beta=2487$ ; $V_r=0.47$ , $u(t)/U_m = 1.22$ .....	47
18e.	Evolution of vorticity. $K=10.5$ , $\beta=2487$ ; $V_r=0.47$ , $u(t)/U_m = 0.47$ .....	47
18f.	Evolution of vorticity. $K=10.5$ , $\beta=2487$ ; $V_r=0.47$ , $u(t)/U_m = -0.29$ .....	47
19a.	Streamlines. $K=10.5$ , $\beta=2487$ ; $V_r=0.47$ , $u(t)/U_m = 0.11$ .....	48
19b.	Streamlines. $K=10.5$ , $\beta=2487$ ; $V_r=0.47$ , $u(t)/U_m = 0.98$ .....	48
19c.	Streamlines. $K=10.5$ , $\beta=2487$ ; $V_r=0.47$ , $u(t)/U_m = 1.46$ .....	48
19d.	Streamlines. $K=10.5$ , $\beta=2487$ ; $V_r=0.47$ , $u(t)/U_m = 1.22$ .....	48
19e.	Streamlines. $K=10.5$ , $\beta=2487$ ; $V_r=0.47$ , $u(t)/U_m = 0.47$ .....	48
19f.	Streamlines. $K=10.5$ , $\beta=2487$ ; $V_r=0.47$ , $u(t)/U_m = -0.29$ .....	48



## LIST OF TABLES

1.	Computed in-line force coefficients for different values of $K$ and $\beta = 1772$ , $V_k = U_o K = 2.05$ .....	25
2.	Computed and experimental in-line force coefficients for different values of $K$ and $\beta = 1772$ , $V_k = U_o K = 4.0$ .....	26
3.	Computed in-line force coefficients for different values of $K$ and $\beta = 1772$ , $V_k = U_o K = 6.05$ .....	26
4.	Computed in-line force coefficients for different values of $K$ and $\beta = 2487$ , $V_k = U_o K = 5.01$ .....	27
5.	Computed in-line force coefficients for different values of $K$ and $\beta = 4122$ , $V_k = U_o K = 2.07$ .....	27



## LIST OF SYMBOLS

$C$	= correlation coefficient between pressure and current velocity.
$C_{il}$	= in-line force coefficient
$C_u$	= transverse (lift) force coefficient
$D$	= diameter
$F_{il}$	= in-line force
$F_u$	= transverse (lift) force
$K$	= Keulegan-Carpenter number = $U_m T/D$
$k$	= surface roughness characteristic dimension
$p$	= pressure
$Re$	= Reynolds number = $U_m D/\nu$
$t$	= time
$T$	= period of oscillation
$u_i$	= velocity in the $i$ direction
$U$	= velocity in the horizontal direction
$U_m$	= velocity amplitude in harmonic flows
$U_o$	= co-linear steady current velocity
$V_r$	= current ratio = $U_o/U_m$
$V_k$	= $KV_r = U_o T/D$
$x$	= horizontal cartesian coordinate
$y$	= vertical cartesian coordinate
$y^+$	= $(y/\nu)(\tau/\rho)^{0.5}$ non-dimensional wall proximity

$\beta$	= frequency parameter = $Re/K$
$\delta$	= Kronecker delta
$\phi$	= arbitrary flow quantity
$\eta$	= dynamic viscosity
$\nu$	= kinematic viscosity
$\rho$	= density
$\tau$	= shear
$\zeta$	=computational grid cell characteristic dimension
$\Delta p_m$	= differential pressure amplitude
$\Delta p_o$	= differential pressure, steady component
$\Delta t$	=time increment

## ACKNOWLEDGEMENTS

There are a number of individuals to whom I would like to express my sincere gratitude for making the completion of this thesis possible. For obvious space constraints, I will limit myself to acknowledging only those whose contributions were most significant.

First among these is Distinguished Professor T. Sarpkaya, who not only imparted on me a fraction of his vast knowledge of fluid mechanics, but also part of his boundless enthusiasm for the subject and a solid appreciation of its importance in our lives.

At several stages along the way, several CFDRC representatives "came to the rescue" when I was not able to solve a software problem on my own. Although others have also made contributions, I would be remiss if I did not mention at least Lyle Johnson, Milind Talpallikar and Fritz Owens for the excellent technical support they provided.

I'd also like to thank Mr. Gary Hufford of CFDRC and Dr Walter Wolfe of the Sandia National Laboratories for sharing some key insight in the area of computational fluid dynamics without which my progress would have been significantly slower.

Finally, I'd like to acknowledge all the friends and members of the Curricular staff who, in many instances, helped me with the more mundane aspects of thesis writing or provided moral support in times of frustration.

## I. INTRODUCTION

The study of time-dependent flows past bluff bodies has historically been the focus of a great deal of scientific attention owing to its relevance to many and diverse applications, ranging from submerged structures to hot wire anemometers. Some forty years ago, Keulegan and Carpenter commenced the methodical investigation of the fluid-structure interactions which occur when bodies are immersed in unsteadily flowing fluids. Today, the effect of the parameters relevant to the problem, such as Reynolds number, Keulegan-Carpenter number and relative roughness, to name a few, is much better understood thanks to ongoing research in this area. In spite of this progress, real time prediction of the forces caused by unsteady flows on submerged objects, such as those acting on an underwater robotic arm or an offshore oil rig, seriously challenges our current theoretical and computational capabilities.

One of the principal empirical tools used by the engineer to solve the problems described above, Morison's equation, is only reliable in predicting forces and moments in highly idealized conditions with very low or very high flow oscillation periods. Additionally, most real-life problems involve flows in the turbulent regime, further increasing the level of difficulty of both analytical and numerical solutions.

Given the cost and complexity of the laboratory apparatus required to reproduce real life flow conditions, theoretical and experimental advances have been paralleled by a considerable research effort in the area of computational fluid dynamics to assist in the solution of problems related to bodies immersed in unsteadily flowing fluids. Progress in numerical techniques and the ever increasing power of present day computers are finally making it possible to overcome the barrier historically imposed by the physical and numerical instabilities which have caused the modelling of turbulent flows particularly challenging in the past.

Whereas, until recently, numerical experimentation has only been successful in determining flow patterns, Strouhal numbers and force coefficients for flow regimes within

selected ranges of relatively low Reynolds numbers, it is now possible to obtain useful data for more turbulent flows exhibiting extensive separation. Furthermore, commercial software is becoming available which affords researchers much greater flexibility than the ad hoc codes previously generated to solve very specific categories of problems, allowing for the analysis of a much broader gamut of flow conditions.

Unfortunately, in spite of such great flexibility, modern software does not yet absolve the user from having to fine-tune the code by the judicious selection of parameters, numerical techniques and turbulence models. Even then, experimentally obtained results cannot be exactly duplicated in all cases.

If complete and accurate solutions are not yet always achievable, however, approximate solutions can certainly aid in expanding our current level of understanding and provide the engineer with a valuable tool to improve design optimization. From the above discussion, it can be inferred that a benchmark body of reliable calculations, performed using the most appropriate set of computation tools, is required to calibrate our current empirical equations and experimental results.

The objective of this investigation is to lay the foundations for such an endeavor and improve our current ability to predict the effects of time-dependent turbulent flows over circular cylinders through the use of a state of the art commercial code generated by CFD Research Corporation (CFDRC). Whenever possible, the results achieved have been compared to those obtained experimentally. Besides their intrinsic value, these results will aid in pointing out some of the strengths and weaknesses of the code and hopefully add to our understanding of the physics of flow types not previously analyzed.

## II. BACKGROUND STUDIES

About twenty years after Keulegan and Carpenter published their ground breaking work, a comprehensive series of experiments concerning sinusoidally oscillating flow about smooth and rough bodies was performed at the Naval Postgraduate School (Sarpkaya, 1976). This endeavor produced a wealth of practical results and introduced the parameter  $\beta$  ( $= Re/K$ ) to assess the influence of scale in periodic flows. Among its findings, the dependence of the force-transfer coefficients on  $Re$ ,  $K$ , and  $k/D$  was shown graphically and amply discussed. As a continuation to this research effort, cases were analyzed which involved a coexisting flow as specified by  $U = U_o - U_m \cos(2\pi t/T)$ , in which  $U_o$  represents the steady mean velocity and  $U_m$  the amplitude of sinusoidal oscillations (Storm 1984). Since the mid-eighties, several numerical predictions of the Strouhal number, the pressure distribution, and the evolution of the lift and drag forces in steady and time-dependent ambient flows have been performed in an attempt to obtain results consistent with experimental data. Here, only the more recent and relevant investigations will be briefly reviewed.

A finite-difference analysis of the Navier-Stokes equations for a sinusoidally oscillating ambient flow about a circular cylinder at  $K = 5$  ( $Re = 1000$ ) and  $K = 7$  ( $Re = 700$ ) has been attempted by Baba & Miyata (1987), assuming a physically unrealistic symmetric wake in both simulations. The results have shown that the calculations could be carried out only for short times (less than two cycles of flow oscillation) with a nonsuper computer.

A similar method was used to analyze three cases ( $K = 5, 7$ , and  $10$ ) at Reynolds numbers around  $10^4$  (Murashige et al. 1989). The flow was perturbed by artificial means to trigger asymmetry. At  $K = 10$ , a transverse vortex street appeared, in agreement with flow visualization experiments.

The transverse vortex street observed at  $K = 12$  was also reproduced correctly and for the first time by Mostafa (1987) using multi-discrete vortices. However, the calculated forces were somewhat larger than those measured.

In later years, numerical experiments with co-existing flows produced extremely

interesting flow features. For relative current velocities  $V_r (=U_o/U_m)$  in the range of 0.7-0.8, the vortices shed nearly symmetrically at each cycle and formed a three-row vortex street in the range of  $V_r = 0.6-0.7$ . For  $V_r$  larger than about one, the vortex wake returned to the asymmetric mode, as in a regular vortex street. Although the scope of this work was limited to relatively low Reynolds numbers, the calculations of resistance in co-existing flows showed that both the inertia and the drag coefficients for  $K = 4-6$  were in reasonable agreement with experimental data (Sarpkaya et al. 1992).

Square cylinders have also been the subject of numerical experimentation. Earlier attempts were flawed by central differencing at large cell Reynolds numbers, which led to spatial oscillations ahead of the rectangle. Improvements were made by using time differencing and third-order upwinding numerical schemes on the convective terms. The technique just described was tried for Reynolds numbers under 3,000 (Davis & Moore 1982). In 1993, Kato and Launder used modified K-epsilon ( $k-\epsilon$ ) and K-omega ( $k-\Omega$ ) turbulence models on square cylinders, further improving the numerical results and obtaining a markedly superior behavior in the near-field region.

Aerodynamic research on airfoils further demonstrated the potential of the  $k-\epsilon$  model. A simulation developed by Rogers (1994), although requiring more grid points than previous ones (such as the Baldwin-Barth model), was significantly better at computing maximum lift conditions and flap boundary-layer separation.

Whereas most of the early numerical codes were generated by higher learning institutions or government research agencies (such as NASA), a number of very versatile computational fluid dynamics (CFD) software, suitable for design and analysis purposes, is currently being produced by the private sector. The code utilized for this investigation is a general-purpose CFD code with multi-domain solution capability issued by CFDRC.

Initial results in applications germane to the subject of the current investigation indicated that the program was capable of predicting Strouhal numbers and forces for uniform flows at higher Reynolds numbers but questioned its ability to capture the high turbulence intensity levels present in the near-wake region (Singhal & Avva 1994). The

program was further tested in uniform flow using the  $k-\epsilon$  and renormalization group (RNG) models at Reynolds numbers over  $10^6$ . Although it was able to predict Strouhal numbers reasonably well, the program was not tested for force coefficients under these flow conditions (Habchi & Hufford 1995).

In the current investigation, the CFDRC software has been used to predict the forces acting on circular cylinders immersed in various types of time-dependent turbulent flows. It is felt that the data presented herein provide a good indication of the code's performance in this application.



### III. NUMERICAL REPRESENTATION

#### A. COMPUTATIONAL METHOD

The CFD-ACE code simulates fluid flow by solving the partial differential equations (PDE) which govern the transport of flow quantities. Since the CFD-ACE theory manual discusses the solution methodology at length, only a brief outline of this topic will be presented here.

The governing equations for the flow conditions investigated are the continuity and Navier-Stokes (NS) equations. For turbulent flows, the code applies Favre (density) averaging to the NS equations, so that each flow quantity  $\phi$  is decomposed into a mean and a fluctuating part according to:

$$\phi = \tilde{\phi} + \phi''; \quad \text{where:} \quad \tilde{\phi} = \frac{\overline{\rho\phi}}{\bar{\rho}} \quad [1]$$

Note that overbar denotes Reynolds (time) averaging, while tilde denotes Favre averaging. Applying the Favre averaging procedure to the continuity and NS equations yields:

$$\frac{\partial \bar{\rho}}{\partial t} + \frac{\partial}{\partial x_j} (\bar{\rho} \tilde{u}_j) = 0 \quad [2]$$

and:

$$\frac{\partial}{\partial t} (\bar{\rho} \tilde{u}_j) + \frac{\partial}{\partial x_j} (\bar{\rho} \tilde{u}_i \tilde{u}_j) - \frac{\partial \bar{\rho}}{\partial x_i} \frac{\partial}{\partial x_j} \left[ \mu \left( \frac{\partial \tilde{u}_i}{\partial x_j} + \frac{\partial \tilde{u}_j}{\partial x_i} - \frac{2}{3} \frac{\partial \tilde{u}_m}{\partial x_m} \delta_{ij} \right) \right] + \frac{\partial}{\partial x_j} (-\bar{\rho} \tilde{u}_i'' \tilde{u}_j'') \quad [3]$$

respectively. By applying the generalized Boussinesq eddy viscosity concept, the Reynolds stresses can be treated as a linear function of the mean strain rate, so the Favre averaged NS (FANS) equation can be expressed as:

$$\frac{\partial}{\partial t}(\bar{\rho}\tilde{u}_j) + \frac{\partial}{\partial x_j}(\bar{\rho}\tilde{u}_i\tilde{u}_j) = -\frac{\partial \bar{p}}{\partial x_i} + \frac{\partial}{\partial x_j}[(\bar{\mu} + \mu_t)(\frac{\partial \tilde{u}_i}{\partial x_j} + \frac{\partial \tilde{u}_j}{\partial x_i} - \frac{2}{3}\frac{\partial \tilde{u}_m}{\partial x_m}\delta_{ij})] - \frac{2}{3}\frac{\partial}{\partial x_i}(\bar{\rho}k) \quad [4]$$

in which  $\eta_t$  represents the turbulent eddy viscosity and  $k$  is half the trace of the Reynolds stress tensor.

In general, except for the continuity, each governing equation can be expressed in a common form comprised of a transient term, a convective term, a diffusive term and a source, not all of which will be present at all times.

The equations corresponding to the flow quantities being analyzed are discretized by the code over finite control volumes and numerically integrated, thereby yielding a set of finite difference equations (FDE). Although algebraic, these FDEs are not linear and are therefore solved using an iterative process.

As mentioned above, there is no governing PDE available for pressure. The task of solving for this flow quantity while satisfying the continuity equation is accomplished by a variation of the "Semi-Implicit Method for Pressure-Linked Equations, Consistent" or SIMPLEC algorithm.

Briefly, the SIMPLEC procedure can be summarized as follows:

1. Estimate the pressure field.
2. Solve for the remaining flow quantities and check whether the continuity equation is satisfied. Since this will not generally be the case, an improved solution will be required.
3. Find correction factors for velocities and density. These can be used to find a correction factor for pressure.

4. Using the correction factor obtained in the preceding step, re-evaluate the pressure and velocity fields.
5. Solve the discretized equations for other flow variables, including turbulence quantities, as required by the specific problem.
6. Repeat steps 2 through 5 until the solution converges.

The aforementioned variation used in the CFD-ACE code consists of repeating steps 3 and 4 a number of times, thus updating the pressure, velocity and density fields prior to proceeding. These intermediate continuity or pressure-correction iterations have been found to enhance overall convergence for most flow problems.

## **B. GRID GENERATION**

The grid used to analyze most models is shown in Figure 1. It was developed using the CFD-GEOM program and is a 1 meter by 1 meter square subdivided into four domains. A circle of diameter 0.05 meters, located at the geometric center of the grid, represents a cylinder of infinite length about which the fluid flows. The internal domain boundaries are located along the diagonals of the square. Sixty-five lines project radially from each of the four quadrants of the circle and meet the sides of the square at equispaced mesh points. Intersecting the radial lines, one-hundred and thirty other lines join mesh points located along the diagonals and spaced such that the grid is much finer in the vicinity of the circle than in the outer regions.

Several requirements were considered during the grid selection process. First, the grid must be sufficiently extensive to prevent any vortices, still strong enough to influence the flow, from migrating beyond the boundaries. Also, while it was recognized that increasing the number of cells (as well as shortening the time interval between iterations) would result in a more accurate vorticity computation, efficiency considerations dictated a

finer mesh only in the vicinity of the cylinder walls, where the effect of vorticity is strongest. Unfortunately, the vortices that separate and are swept away diffuse rapidly as the mesh coarsens, resulting in returning vortices which are probably weaker in the model than they would be in actuality.

When the number of grid cells was quadrupled, marginal improvements in the results were obtained at the cost of a four-fold increase in CPU time. It was felt, therefore, that the grid just described represented the best compromise between accuracy and computation efficiency.

### **C. BOUNDARY CONDITIONS**

In the CFD-ACE program, boundary conditions can be specified via drop-down menus or by editing the file in which all flow parameters are stored. Since this file has an ".in" suffix, it will hereinafter be referred to as in-file.

Four types of boundary conditions are used in all the simulations performed. The top and bottom sides of the flow region are designated as symmetry boundaries. This condition implies a zero normal velocity and a vanishing gradient normal to the boundary for all variables.

Each cylinder quadrant is designated as a wall, implying, again, a zero normal velocity along the boundary.

The vertical sides of the square, referred to as east and west boundaries, are both designated as exits with prescribed pressure, resulting in a paradoxical flow region with two outlets and no inlet. This apparent anomaly, present in all time-dependent flow simulations performed, can be explained by pointing out a peculiarity of the code nomenclature: while boundaries designated as inlets do not allow bidirectional flow, exits do. Several other inlet and exit conditions may be specified to accomodate supersonic, compressible and other types of flow.

It should be noted that the flow conditions need not be the same along the entire length of each boundary. It is possible, for instance, to specify a higher flow velocity at

the northern half of an inlet or exit and a lower one along the southern half. This technique was found particularly useful when flow perturbations were desired to precipitate the asymmetrical shedding of vortices in uniform flow.

A fourth type of boundary, called interface, is utilized to designate lines along which one domain meets with another within the flow region.

#### D. FLOW CONTROL

In the CFD-ACE program, velocity at an inlet or exit boundary can be specified either as a constant or as one of a limited number of time-dependent functions. Pull-down menus can be used to specify constant flows while time-dependent flows must be specified by editing the in-file.

In the simulations performed, it was desired for the ambient velocity to vary as:

$$U(t) = U_0 - U_m \cos \frac{2\pi}{T} t \quad [5]$$

in which  $U_0$  represents a steady component, i.e., a current, and  $U_m$  the magnitude of the fluctuating component. Unfortunately, velocity was noted not to follow harmonic functions whenever such a function was invoked. CFDRC personnel acknowledged this anomaly although its underlying causes were not discussed.

Flow can also be controlled by making use of the following relationship between pressure and velocity:

$$-\frac{dp}{dx} = \frac{2\pi}{T} \rho U(t) \quad [6]$$

and by prescribing a time-dependent pressure at the exits. It can be shown that, if velocity

is to vary cosinusoidally, the amplitude of the differential pressure should be:

$$\Delta p_m = \frac{2\pi}{T} \rho U_m \Delta x \quad [7]$$

where  $\Delta x$  is half the length of the flow region. The amplitudes specified at the east and west exits should be equal in magnitude and opposite in sign. Since pressure and velocity are offset by  $\pi/2$  radians by virtue of Equation [6], differential pressure should vary sinusoidally, resulting in a pressure which varies linearly in space while its slope varies harmonically in time.

The technique just described allows the user to calculate the magnitude of the oscillating differential pressure required to generate the desired flow velocity. Whenever a current is present, however, a steady differential pressure is also required. It was empirically determined that this steady component is defined as:

$$\Delta p_0 = \frac{1}{2} \rho U_m^2 V_r C ; \text{ where } V_r = \frac{U_o}{U_m} \quad [8]$$

in which  $C$  is dependent on  $K$  and on the time step used. The manner in which this constant was evaluated, as well as some recommended values for different  $K$  ranges and a time step of 0.02 seconds are discussed in Appendix B.

## **E. DATA REDUCTION AND CALCULATION OF FORCE COEFFICIENTS**

Once the program algorithm has converged on a set of numerical values for the flow quantities sought at each time step, the results are recorded in a file whose suffix is ".out" and will therefore be referred to as the out-file.

In order to reduce the data to a useful format, it was found necessary to transfer the numerical results pertinent to the investigation from the out-file to a new file. Since the

code calculates shear and pressure forces separately at each boundary designated as a wall, it is helpful if in the course of data transfer the contributions from each wall were consolidated into a single value for each cartesian axis.

Once the total horizontal and vertical forces are available, in-line force and lift coefficients are obtained as follows:

$$C_{il} = \frac{\Sigma F_{il}}{0.5\rho U_m^2 D} \quad [9]$$

and:

$$C_l = \frac{\Sigma F_l}{0.5\rho U_m^2 D} \quad [10]$$

It is also possible for the code to record a given flow quantity at a specified point and tabulate the results in a monitor file. Both flow quantity and location to be monitored must be specified by the user. This capability was used extensively to record velocities in order to verify and later fine-tune the flow control technique described in an earlier section.

Once the desired coefficient or flow quantity is tabulated, its trend can be plotted and further analyzed using one of several commercially available codes.

## F. INPUT OPTIONS

The CFD-ACE Command Language Manual describes the basic techniques used to specify the code inputs and the other computational options available. Although drop-down menus can be used in most cases, certain types of inputs can only be specified by editing the in-file. This section will concentrate on specific aspects of input definition which were found particularly relevant and in some cases critical to the type of flow conditions

investigated. A sample in-file with useful comment is presented in Appendix C.

A very important aspect of flow control is the proper definition of the coefficients in the harmonic functions which determine the pressure differential across the flow region. Of these coefficients, C1 represents the steady state component ( $\Delta p_0$  in Equation [8]), C2 the amplitude of the sinusoidally oscillating component ( $\Delta p_m$  in Equation [7]), and C3 its frequency in radians per second. The remaining coefficients, C4 and C5, were set to zero as they are used for cosinusoidal components, not present in any of the cases examined.

The user must specify an initial and a final time for all time-dependent flows. The time increment is indirectly specified by inputting the number of time steps to be used and should be chosen taking into account the fineness of the grid mesh and the flow velocity. In general it is not desirable to have the fluid travel a distance greater than half of a cell during a single time step. Luckily, a modicum of experimentation can quickly reveal whether the improvement in output quality is worth the longer computation time required when the time step is shortened.

It should be noted that it may be desirable for the initial time to differ from zero because the program has the capability of restarting from a set of initial conditions recorded at the end of a previous run, allowing for two sets of output data to be spliced together and plotted continuously versus time.

The solution control part of the in-file is one where the available options must be chosen judiciously and some trial and error may be required. In most cases, the default upwind spacial differencing scheme and Euler temporal scheme will work satisfactorily. Some preliminary testing of other options led to the observations which follow.

Use of the Crank-Nicholson scheme cannot be prescribed using the appropriate drop-down menu as this will result in a syntax error within the in-file. In general, however, this technique does not produce appreciable changes with respect to the results achieved using the default Euler method.

While the upwind spacial differencing method is very robust, central differencing may become unstable, especially when used in conjunction with fine grid meshes. This

problem can usually be overcome by the appropriate selection of a blending factor: in most models in which central differencing was used, a blending factor of 0.3 was specified; 0.5 was successfully substituted in models which diverged. The greater the blending factor, the more the technique will have an upwind character.

Other spatial differencing schemes did not work satisfactorily on the type of computer used. A later version of the program corrected this.

The number of solution iterations and sub-iterations for each flow quantity can only be selected using some experimentation or previous experience and it will differ for each type of problem analyzed. In general, all iterative processes should be shortened as much as possible without compromising accuracy. This can only be done by solving a problem with a known solution and changing the number of iterations until a satisfactory result is obtained. The program allows for visualization of the trend in the residuals of each flow quantity calculation, so the slope of residual graphs is also helpful in determining the optimum number of iterations.

The code offers a choice of six different turbulence models, only three of which were utilized in the course of this investigation. The standard  $k-\epsilon$  model was found to work satisfactorily in most circumstances. Very minor changes were noted in the output when the RNG model was used. Whenever the grid-flow velocity combination is such that  $y^+ (= (y/v)(\tau/\rho)^{0.5})$  is smaller than about 11 at the grid cell center closest to the cylinder wall, use of the Low Reynolds model is appropriate and results in better numerical accuracy. Since in time-dependent flows velocity varies, the user needs to determine whether the values of  $y^+$  warrants selecting the Low Reynolds model. All the above models require the user to input two parameters, turbulence kinetic energy and turbulence length scale. It was found that varying the former from a value corresponding to 3% to 10% turbulence caused minimal changes in the results, so 3% was used throughout. The latter was varied between  $0.09 D/2$  and  $0.09 D$  ( $D$  being the cylinder diameter) without noting significant differences.



## IV. DISCUSSION OF RESULTS

### A. INTRODUCTION

The results will be presented in the following order. First, a discussion of the grid and other code inputs used in the calculations. Second, a detailed discussion of the in-line and transverse force coefficients as functions of the selected governing parameters. Finally, a comparison, whenever possible, of the calculated and experimental values. This section is then completed with plots of vorticity and streamlines for representative values of flow parameters. Throughout, a special attempt is made to concentrate on the most informative range of the calculations rather than on a massive presentation of the data.

### B. GRID AND INPUT PARAMETERS

As discussed in Section III B, the code used allowed one to generate various types of grids. For the problem under consideration, the axial symmetry of the cylinder, the problem's two-dimensionality and oscillating nature (left and right boundaries), and the extreme importance of the accurate calculation of the velocity gradients at and near the cylinder surface were kept in mind. Several trials and tribulations finally resulted in the grid shown in Fig. 1. It consists of four domains. The smallest cell size is  $3.05 \times 10^{-5} D$  along the circumference of the cylinder and  $2.56 \times 10^{-5} D$  in the radial direction. The largest cell, at the outer boundaries, is  $0.313 D$  by  $0.245 D$ . The size of the computational domain is  $20 D$  by  $20 D$ .

Careful consideration had to be given to the selection of the grid size for reasons beyond the accurate calculation of the velocity gradient on the cylinder. The fact that the flow oscillates makes the vortices generated during one half-cycle return toward their inception point. Thus, if a vortex does not retain its integrity as it transits areas of coarser mesh, then it will return to the cylinder with artificial diffusion above and beyond that imposed by the prevailing turbulence. Furthermore, the stability of the flow, regardless of where the cell may be, is dictated, among other parameters, by the Von Neumann criterion.

It states that flow at a given point should not displace more than one half of the cell on which the fluid particle resides. This is a difficult condition to satisfy even in unidirectional steady flows. Since in periodic flows, with or without current, the magnitude of the ambient velocity fluctuates between zero and a prescribed maximum, then one either allows violation of the Von Neumann criterion at times of peak velocity, so that global instability is not allowed to dominate the flow, or is penalized in terms of grid fineness, and consequently CPU time, by satisfying the criterion throughout. The experience of others, as well as the present one have demonstrated that the latter is impractical.

In the present simulations, a compromise was made to maintain sufficient accuracy while sacrificing neither physics nor a reasonable CPU time. It is as a result of the foregoing considerations that the quantity  $U_m \Delta t / \zeta$ , where  $\zeta$  is the grid cell's characteristic length, was allowed to reach values on the order of 50 in the vicinity of the cylinder walls. It should be noted, of course, that the quantity  $u(t) \Delta t / \zeta$ , i.e. the ratio of the actual distance traveled by the fluid to the computational cell's characteristic length, is expected to be substantially less than  $U_m \Delta t / \zeta$  in the immediate vicinity of the solid wall boundary.

In the results to be presented, the flow parameters chosen were the Keulegan-Carpenter number  $K$ , the relative velocity parameter  $V_r$  and the frequency parameter  $\beta$  or the Reynolds number  $Re$ . The majority of the calculations were performed with a time interval  $\Delta t$  of 0.02 seconds. As will be noted in connection with the sensitivity analysis discussion, the time interval, and other code and problem related parameters, such as the turbulence models, were judiciously varied. It is fully realized that a numerical simulation, like a physical experiment, produces only a data point on the basis of the input parameters chosen and discretization schemes employed in the code. Thus, the insight that one develops through familiarity with the phenomenon is brought to bear on the selection of the input parameter and on the comparison of the results with those obtained experimentally. While the calculations undoubtedly suffered from boundary constraints and artificial diffusion, the experiments have their own corresponding limitations with more or less uncertainties.

Once the parameters were chosen, the code was capable of producing the in-line and

transverse forces and the necessary information for the plot of vorticity and streamlines. The calculations have been carried out for a minimum of seven and a maximum of 30 cycles.

### C. IN-LINE AND TRANSVERSE FORCE COEFFICIENTS

These will be discussed for  $\beta = 1772$ , 2487, and 4122. In case of  $\beta = 1772$ , the analysis was carried out for six  $V_r$  values, corresponding to six  $K$  values ranging from 8.6 to 36. For  $\beta = 2487$ , for five  $V_r$  values corresponding to five  $K$  values ranging from 10.5 to 46. Finally, for  $\beta = 4122$ , for three values of  $V_r$ , corresponding to three values of  $K$  ranging from 5.2 to 24. In addition, for  $\beta = 1772$  only, the parameter  $V_k (= KV_r = U_0 T/D)$  was assigned three different values in order to compare the results with those obtained experimentally wherever possible. For the other two  $\beta$  values, only single values of  $V_k$  were used. In fact, it is because of this reason that there was a one-to-one correspondence between  $V_r$  and  $K$  for each combination of  $\beta$  and  $V_k$ .

Figures 2a through 2d show the in-line force coefficient ( $C_{il}$ ) and the transverse force coefficient ( $C_{it}$ ) for  $\beta=1772$ ,  $K=8.6$  and  $V_k=2.05$ . The basic difference between the first two and the second two figures is that the former were produced using the  $k-\epsilon$  turbulence model and the latter using the low Reynolds number (Low-Re) model. The purpose of this exercise was to demonstrate the consequences of the use of two turbulence models.

It is realized that, for the case being discussed, the maximum  $Re$  is approximately 15,000 and that, during any given cycle, the flow undergoes a transition from laminar to turbulent. Thus, the use of a turbulence model such as the  $k-\epsilon$ , tailored for use in high  $Re$  steady flows, may not be entirely appropriate for an unsteady flow at relatively low  $Re$ . A comparison of Figs. 2a and 2c shows that, whereas in the former  $C_{il}$  does not have an inflection point even as late as the fourth cycle, in the latter an inflection point is evident shortly after the first cycle. The fact that the evolution of the inflection point is directly related to the occurrence of asymmetric vortex shedding is an indication of the evolution of the lift force. In fact, a comparison of Figs. 2b and 2d shows that there is no significant lift in the former relative to the latter. In other words, the use of the Low-Re model, thought to

be more appropriate for low Re flows, gives rise to transverse force and vortex shedding after a few cycles from the inception of flow.

A comparison of the turbulence models cannot be made for all the cases considered in this study because of obvious time limitations. Nevertheless, an effort is made to combine such sensitivity analyses into a section to be presented later.

Returning to the presentation of the results, and in particular to the case of  $\beta = 1772$ , Figs. 3 and 4 show the  $C_{il}$  for  $V_k=2.05$  for  $K=15$  and  $36.5$ . It is evident from a brief perusal of these figures that the in-line force assumes a quasi-steady state within four to six cycles. The shape of the  $C_{il}$  graph, particularly in Fig. 4, is reminiscent of an odd harmonic function, with the inflection points near the upper left and the lower right of each cycle associated, as noted earlier, with the alternate shedding of the vortices from the top and bottom of the cylinder.

Figures 5a, 6a, 6c and 7 show  $C_{il}$  again for  $\beta=1772$  for  $V_k=4$  and for three different  $K$  values. The most noteworthy among the four plots is Fig. 6a, where  $C_{il}$  exhibits irregular behavior after approximately eight cycles, having earlier reached a quasi-steady state. This seemingly strange occurrence is due to the phenomenon known as the transverse vortex street. For  $K$  values in the range of  $10 < k < 13$ , the vortices shed from the cylinder move in the transverse direction and only on one side of the cylinder. This means that the vortices shed in each cycle go around the cylinder and find their way in the positive or negative vertical direction, thereby creating asymmetrical and unsteady in-line forces. This phenomenon has been discussed in detail by Sarpkaya and Isaacson (Sarpkaya and Isaacson, 1981). In fact, Fig. 6b shows that a transverse force develops after approximately seven cycles and reflects the shedding of the vortices at the top and bottom of the cylinder for a number of cycles. It should be noted that Figs. 6a and 6b were developed using the renormalization group theory (RNG) turbulence model, whereas the low-Re model was used to generate Figs. 6c and 6d. Even though the  $C_{il}$ 's do not differ significantly, the transverse force coefficients ( $C_{il}$ ) show the dramatic effect of the choice of turbulence model used in the evolution of the vortex asymmetry. As will be noted later, not all predictions of different

turbulence models will yield the same result even when the same set of governing parameters is used.

Figures 8 and 9a show  $C_{il}$ , again for  $\beta=1772$ , for a higher value of  $V_k$  and for  $K=10.3$  and 36.5. Figure 9a is particularly interesting in that  $C_{il}$  is asymmetrical in shape and magnitude even though  $K$  is as large as 36.5. Normally, one would expect a steady flow like behavior for  $V_k=0$  and relatively large  $K$  values. An examination of Figs. 9a and 9b indicates that neither  $C_{il}$  nor  $C_{tl}$  are symmetrical in the presence of a current, whereas Figs. 9c and 9d, which correspond to flows with no current but otherwise at identical values of  $K$  and  $\beta$ , show that both  $C_{il}$  and  $C_{tl}$  are as symmetrical as they can be after an initial stage of flow development. Thus, the presence of current has a significant impact on the topology of vortex shedding although the superposition of collinear waves and current do not necessarily lead to periodically alternating vortex shedding. It is because of this reason that  $C_{il}$  in Fig. 9a exhibits symmetry neither in magnitude nor in shape.

The next case to be considered is for an intermediate  $\beta$  value of 2487. Figures 10 through 12 show  $C_{il}$  for  $V_k=5.01$  and for three values of  $K$ . The most significant aspect of the graphs is that the amplitude of the oscillation decreases with increasing  $K$  and the shape of the  $C_{il}$  trace becomes less sinusoidal, reflecting, at each half cycle, the asymmetric shedding of the vortices.

Figure 13 shows the  $C_{il}$  for the highest  $\beta$  value dealt with in this investigation for  $V_k=2.07$ . The force oscillations are, as expected, fairly sinusoidal since, for small  $K$  values, one does not expect significant vortex shedding.

Figures 14a and 14b for  $V_k=2.07$  and  $\beta=4122$  shows what happens to in-line and lift forces in the most dramatic range of  $K$ . When  $K$  is in the range between 10 and 20, vortex shedding becomes very chaotic,  $C_{tl}$  decreases significantly and  $C_{il}$  drops down relative to the case of  $K=5$ .

The presence of current further complicates the flow topology with respect to the no-current case in this most sensitive region of the  $K$  values. The flow does not have any sort of symmetry about either axis. Even though the prediction of forces in this region is rather

difficult, there is one beneficial effect deriving from the smallness and the chaotic character of the lift, i.e. the minimization or practical elimination of the tendency of the cylinder to develop a dynamic response or hydroelastic oscillations. However, for  $K=24$  ( $\beta=4122$  and  $V_k=2.07$ ), the vortex shedding becomes quasi-periodic and the  $C_d$  increases considerably as shown in Figs. 15a and 15b.

A harmonic analysis of the lift coefficient has shown that the ratio of the frequency of vortex shedding to the flow oscillation frequency is in the range of 3 to 4 depending on  $V_k$ . Such an analysis is not shown here but may be found in Storm's work. (Storm, 1984).

#### **D. FLOW VISUALIZATION**

Figures 16a through 16f show the evolution of vorticity for  $K=8.78$  and  $\beta=1772$ . In this particular flow regime, vortices are formed and shed from the body in quasi-symmetrical pairs, so that no significant amount of lift is generated. This observation is reinforced by examining Figs. 17a through 17f, which show the streamlines corresponding to the same flow regime.

Figures 18a through 18f show the more complex flow topology resulting from a slightly higher  $K$  and a much higher  $\beta$ . (10.5 and 2487 respectively). The corresponding streamlines, shown in Figs. 19a through 19f, clearly indicate that the vortex pattern is asymmetrical, so that a sizable lift force results.

#### **E. NUMERICAL RESULTS**

The values of the maximum in-line force coefficients and the corresponding governing parameters are listed in Tables 1 through 5. Unfortunately, experimental results were available only for one set of the governing parameters. The general trends noted are that the agreement with both the Morison's equation and with experimental data is better for  $K$  values less than about 10 and larger than 20. This confirms that in a  $K$  range close to that in which a transverse vortex street can be expected to develop, the flow topology is particularly challenging to capture. Another trend noted was that, as the value of  $V_k$

increases, the agreement between the computed  $C_{ii}$  values and those produced by the Morison's equation will deteriorate slightly. The availability of additional experimental data at higher  $V_k$  would be required to draw more insight from the observed trend.

#### F. SENSITIVITY ANALYSIS

A fairly detailed sensitivity analysis for no-current cases was conducted by Hanson (Hanson, 1995). Since in that investigation the same computational grid, turbulent parameters, and time increment were used as those employed in this study, most of the findings are valid for the cases examined herein.

The analysis conducted within the scope of this work involves primarily turbulent models and time increments. Since, due to time constraints, this analysis was performed on representative cases only, some of the observations made will be mostly qualitative in nature.

In all cases examined, the turbulence parameters prescribed corresponded to 3% turbulence and an integral turbulent length scale of 0.00225. The fluid density was 998 Kg/m<sup>3</sup> and the kinematic viscosity  $1 \times 10^{-6}$  m<sup>2</sup>/s. A spacial central differencing scheme with a blending factor of 0.3 was used, along with an Euler temporal scheme. Other computational parameters can be obtained from Appendix C, which is a fairly typical in-file.

Several turbulence models were tested for the case corresponding to  $K=12.19$ ,  $\beta=1772$ ,  $V_k=4$ . While these all produced values of  $C_{ii}$  within 3% of each other, the  $k-\epsilon$  model produced no inflection point after the second oscillation and the vortex pattern appeared to be still symmetrical after 7 cycles of flow oscillation. In contrast, the traces produced by the RNG and Low Re models are shown in Figs. 6a through 6d.

As previously stated, the quantity  $U_m \Delta t / \zeta$  was allowed to reach values in excess of 50 at the cylinder walls. The case corresponding to  $K=24$ ,  $\beta=4122$  ( $Re=100,000$ ), for which the initial value of  $U_m \Delta t / \zeta$  was 62.3 was examined as it represents one of the highest values of that quantity encountered in this study. The time increment was first adjusted so that  $U_m \Delta t / \zeta$  was approximately 12.5. This resulted in a reduction in  $C_{ii}$  from 1.22 to 1.05. (A similar procedure for  $K=46$  and  $\beta=2487$  resulted in a reduction in  $C_{ii}$  from 1.1 to 0.8.) A

further reduction in  $U_m \Delta t / \zeta$  to 0.623 did not result in a sizeable change with respect to the case corresponding to  $U_m \Delta t / \zeta = 12.5$  (less than 1%). Very little effect on  $C_{ii}$  (<2%) was also noted when  $U_m \Delta t / \zeta$  was changed from approximately 15 to less than 0.5 for a case where  $K=12.19$  and  $\beta=1772$ .

It is reasonably safe, therefore, to conclude that, for the particular computational grid used, values of  $U_m \Delta t / \zeta$  on the order of 15 should be acceptable. Although there is not sufficient data to pinpoint the critical value of  $U_m \Delta t / \zeta$  for which a significant impact on the result should be expected, this value will almost certainly be between about 20 and 50.

**TABLE 1**

Computed in-line force coefficients for different values of  $K$  and  $\beta = 1772$ ,  
 $V_k = U_o K = 2.05$

$K$	$V_r$	$C_{il}$ (calc.)	$C_{il}$ (Morison)
8.6	0.22	<u>2.39</u>	2.37
12.1	0.16	<u>1.75</u>	2.12
15.0	0.14	<u>1.49</u>	1.85
17.8	0.12	<u>1.31</u>	1.66
25.8	0.09	<u>1.05</u>	1.30
36.5	0.07	<u>0.92</u>	1.08

**TABLE 2**

Computed and experimental in-line force coefficients for different values of K and  $\beta=1772$ ,  
 $V_k = U_o K = 4.0$

K	$V_r$	$C_{il}$ (calc.)	$C_{il}$ (Mor)	$C_{il}$ (Exper)
8.78	0.43	<u>2.39</u>	2.78	2.60
12.19	0.31	<u>1.83</u>	2.42	2.25
17.82	0.23	<u>1.33</u>	1.87	1.70
26.07	0.16	<u>1.09</u>	1.43	1.10

**TABLE 3**

Computed in-line force coefficients for different values of K and  $\beta = 1772$ ,  
 $V_k = U_o K = 6.05$

K	$V_r$	$C_{il}$ (calc.)	$C_{il}$ (Mor)
10.3	0.56	<u>2.11</u>	3.56
12.1	0.49	<u>1.84</u>	3.17
25.8	0.25	<u>1.14</u>	1.61
36.5	0.18	<u>1.02</u>	1.31

**TABLE 4**

Computed in-line force coefficients for different values of  $K$  and  $\beta = 2487$ ,  
 $V_k = U_o K = 5.01$

$K$	$V_r$	$C_{il}$ (calc.)	$C_{il}$ (Mor)
10.5	0.47	<u>2.10</u>	3.05
12.4	0.40	<u>1.84</u>	2.56
17.2	0.30	<u>1.48</u>	1.86
29	0.19	<u>1.18</u>	1.14
46	0.13	<u>1.10</u>	0.81

**TABLE 5**

Computed in-line force coefficients for different values of  $K$  and  $\beta = 4122$ ,  
 $V_k = U_o K = 2.07$

$K$	$V_r$	$C_{il}$ (calc.)	$C_{il}$ (Mor)
5.1	0.41	<u>4.14</u>	3.44
15	0.14	<u>1.58</u>	1.33
24	0.11	<u>1.22</u>	0.97



## V. CONCLUSIONS

The purpose of this investigation was a critical assessment of the numerical analyses of two-dimensional, sinusoidally oscillating, turbulent flows at relatively large  $Re$ ,  $K$  and  $V_r$ . A number of turbulence models, including the standard  $k-\epsilon$ , RNG based  $k-\epsilon$ , and Low- $Re$  models have been employed. The emphasis was on the validation and accuracy of the time-dependent computations. Observations relating to both numerical and physical validation lead to the following remarks:

- (1) The finite differencing formulation of the Favre Averaged Navier Stokes equation (FANS) can reasonably solve flows within a wide range of  $Re$  using a modified SIMPLEC method. However, the predicted forces will almost always be smaller than those obtained experimentally.
- (2) The turbulence models used do not fully capture vortex strength and prematurely dissipate the vortices relative to experimental observations and measurements. All models used herein (standard  $k-\epsilon$ , RNG based  $k-\epsilon$ , and Low- $Re$  models) fail to predict accurately the exact size of the vortices and the high turbulence intensity levels present in the near-wake of time-dependent flows (subjected to unsteady pressure gradients). This is the primary cause of the aforementioned tendency to underpredict the force coefficients.
- (3) The use of much finer grids, reduced time increments and higher-order spacial and temporal differencing schemes (at the expense of increased CPU time) will not always increase the accuracy of the predictions since the validity of the turbulence models for flows subjected to extra strains such as the time-dependent pressure gradients remains unknown.
- (4) Turbulence is at present, and is likely to remain for a long time, the greatest roadblock to computational fluid dynamics. Some appreciation of the incomplete knowledge bases (both numerical and experimental), retrofitting of data, and the assessment of their consequences are necessary to achieve often qualitative and occasionally quantitative simulations, particularly in time-dependent flows. This is a compromise between expectations and achievables and between physically relevant dynamics and specific quantitative results.



## APPENDIX A. FIGURES

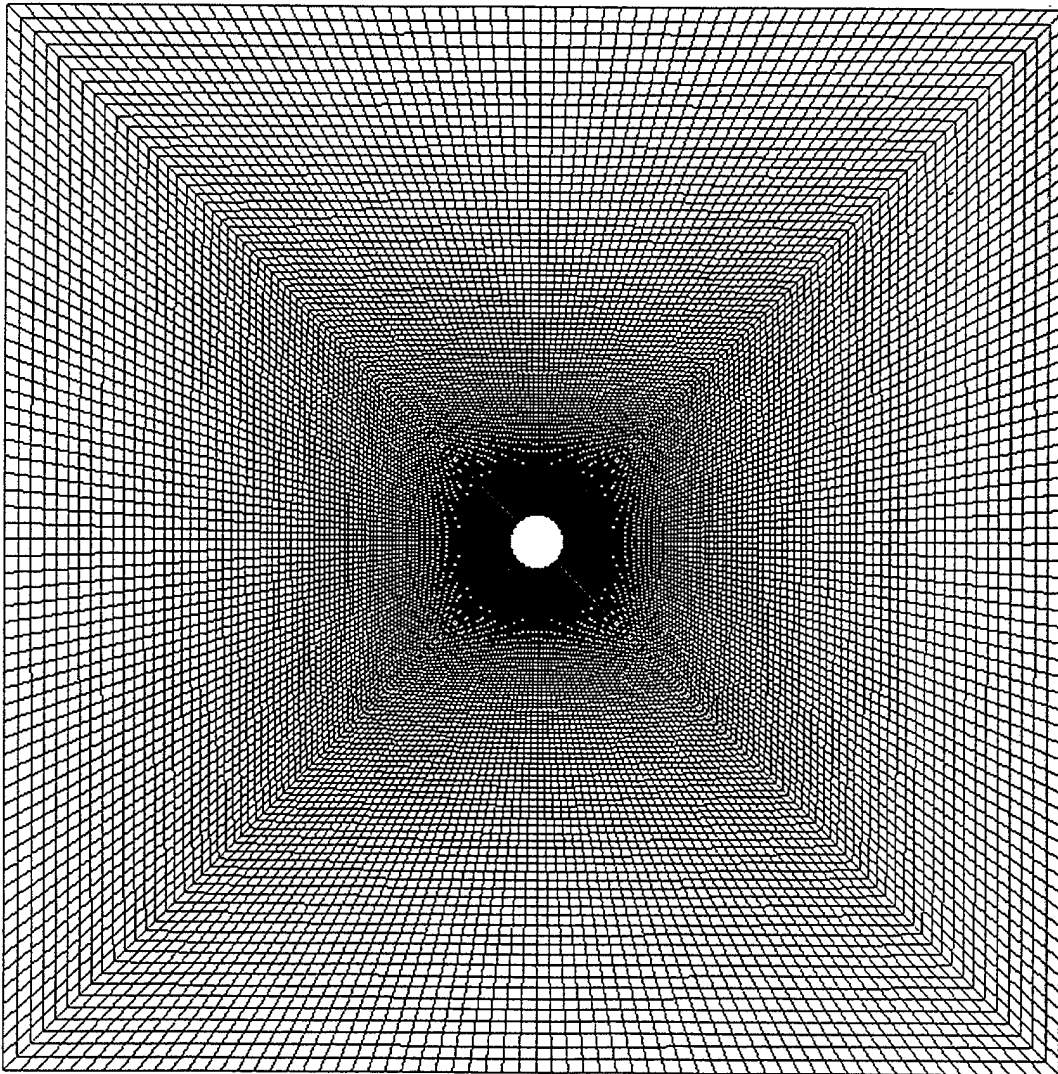


Figure1. Computational Grid.

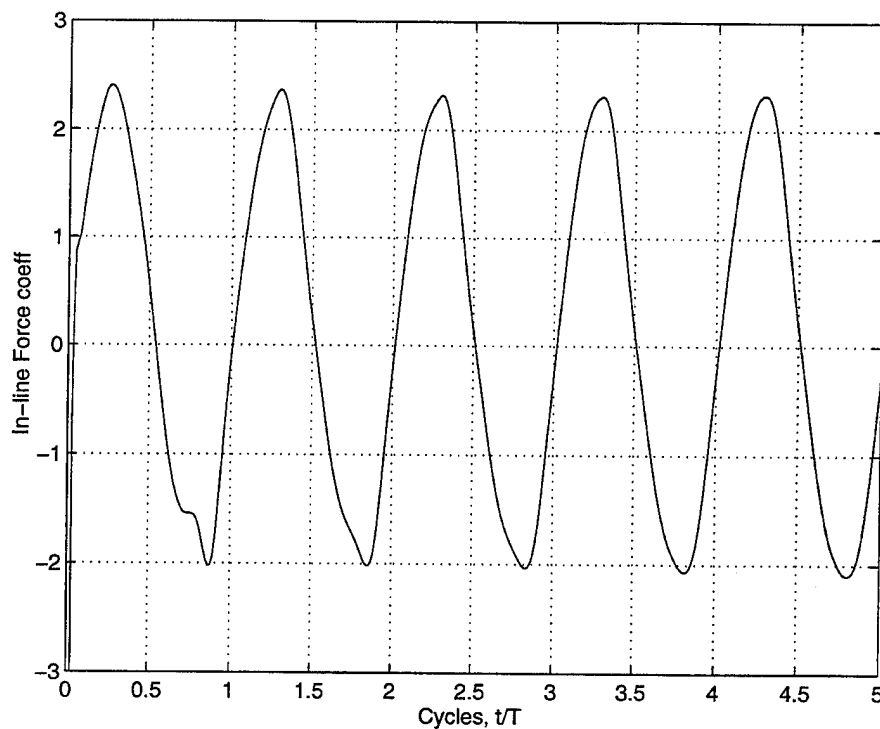


Figure 2a. In-line force coefficient versus time.  $K=8.6$ ;  $\beta=1772$ ;  $V_k=2.05$   
( $k-\epsilon$  turbulence model used)

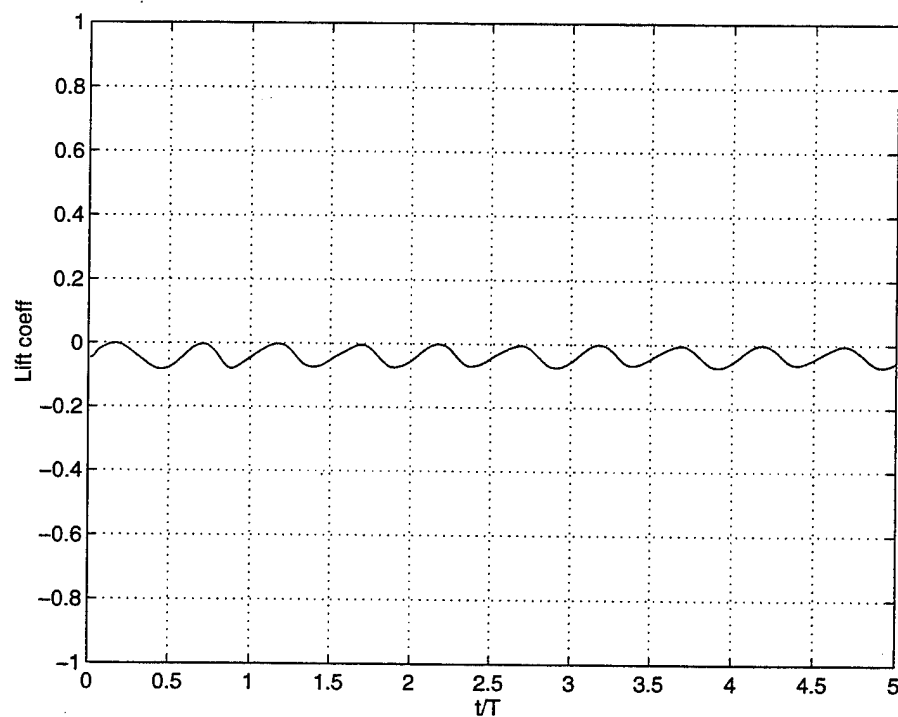


Figure 2b. Transverse force coefficient versus time.  $K=8.6$ ;  $\beta=1772$ ;  $V_k=2.05$   
( $k-\epsilon$  turbulence model used)

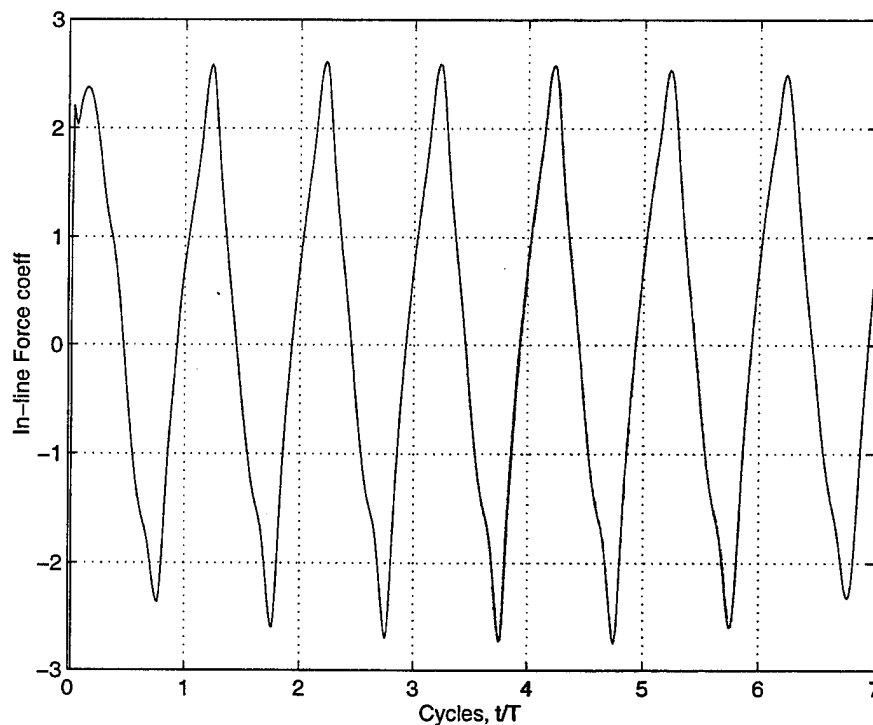


Figure 2c. In-line force coefficient versus time.  $K=8.6$ ;  $\beta=1772$ ;  $V_k=2.05$   
(Low Re turbulence model used)

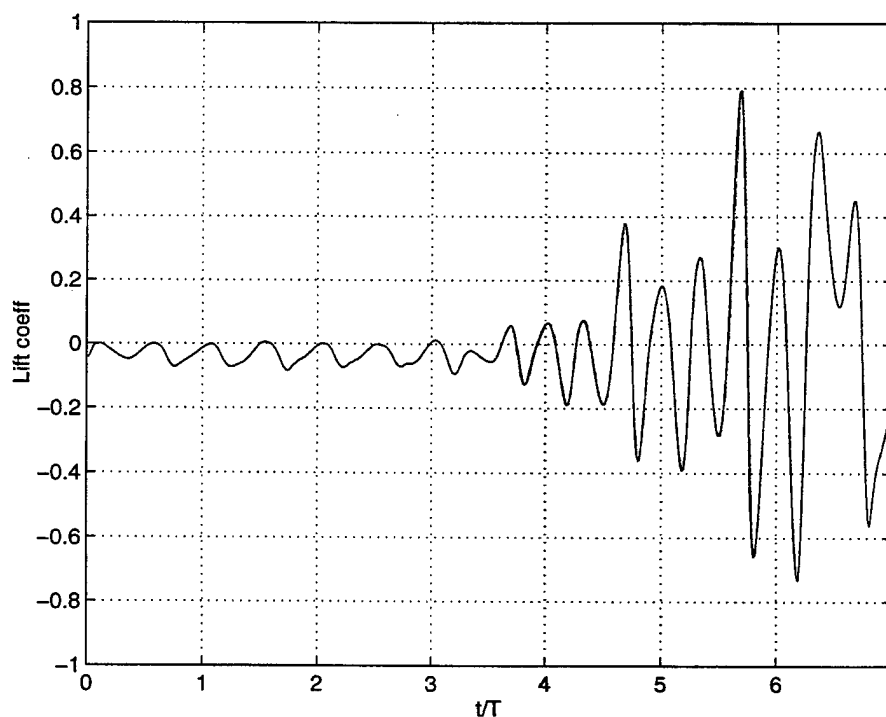


Figure 2d. Transverse force coefficient versus time.  $K=8.6$ ;  $\beta=1772$ ;  $V_k=2.05$   
(Low Re turbulence model used)

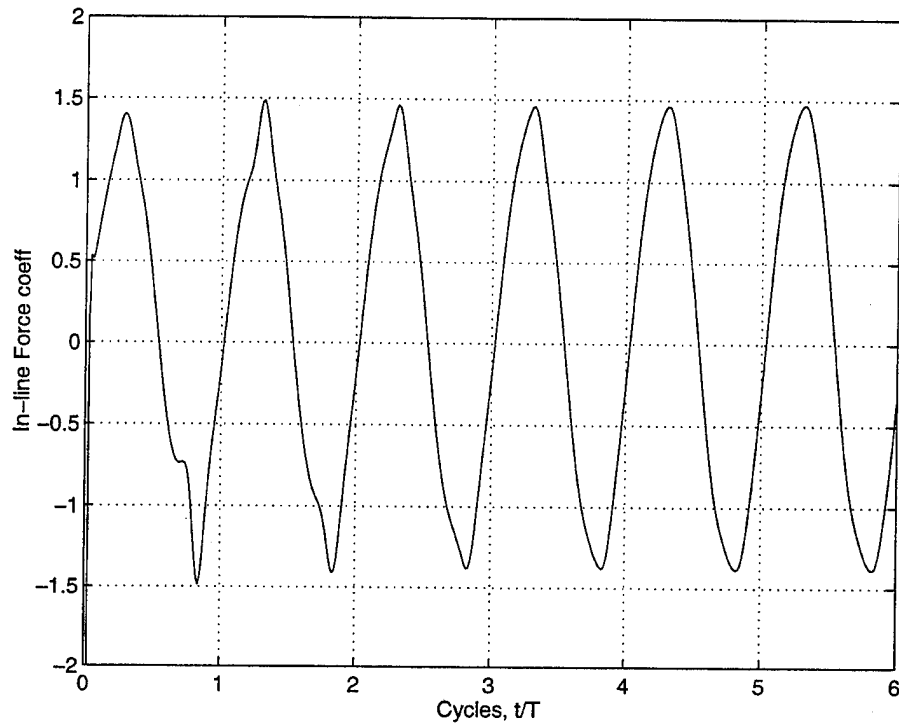


Figure 3. In-line force coefficient versus time.  $K=15$ ;  $\beta=1772$ ;  $V_k=2.05$

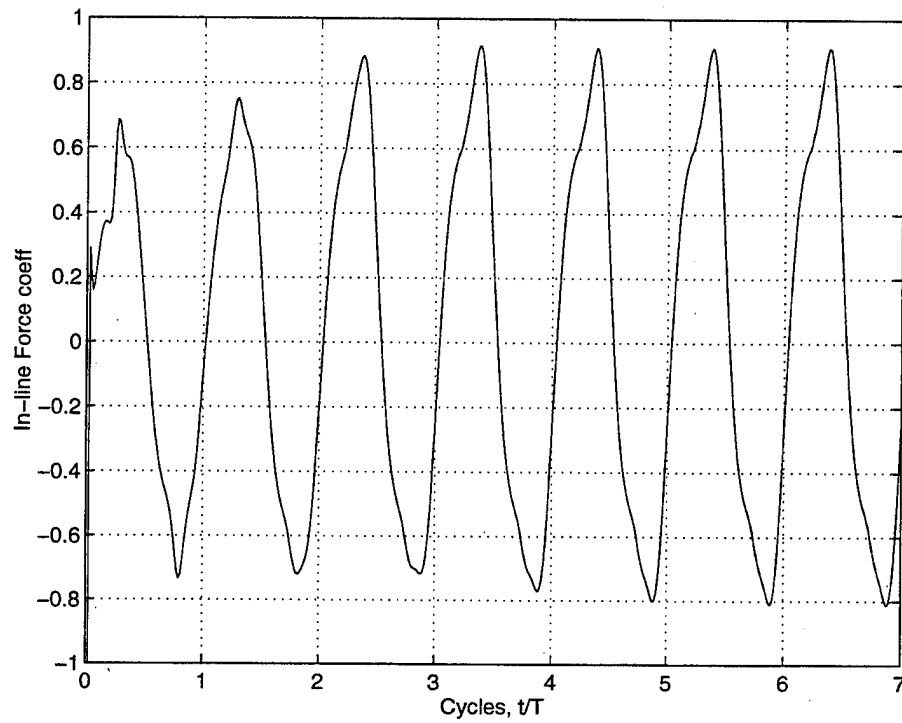


Figure 4. In-line force coefficient versus time.  $K=36.5$ ;  $\beta=1772$ ;  $V_k=2.05$

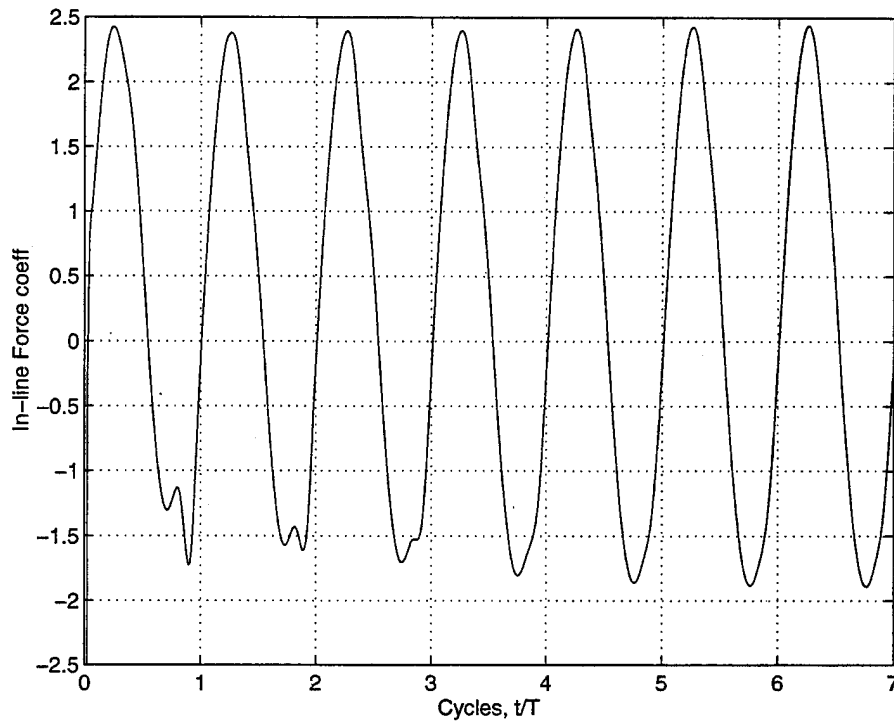


Figure 5a. In-line force coefficient versus time.  $K=8.78$ ;  $\beta=1772$ ;  $V_k=4$

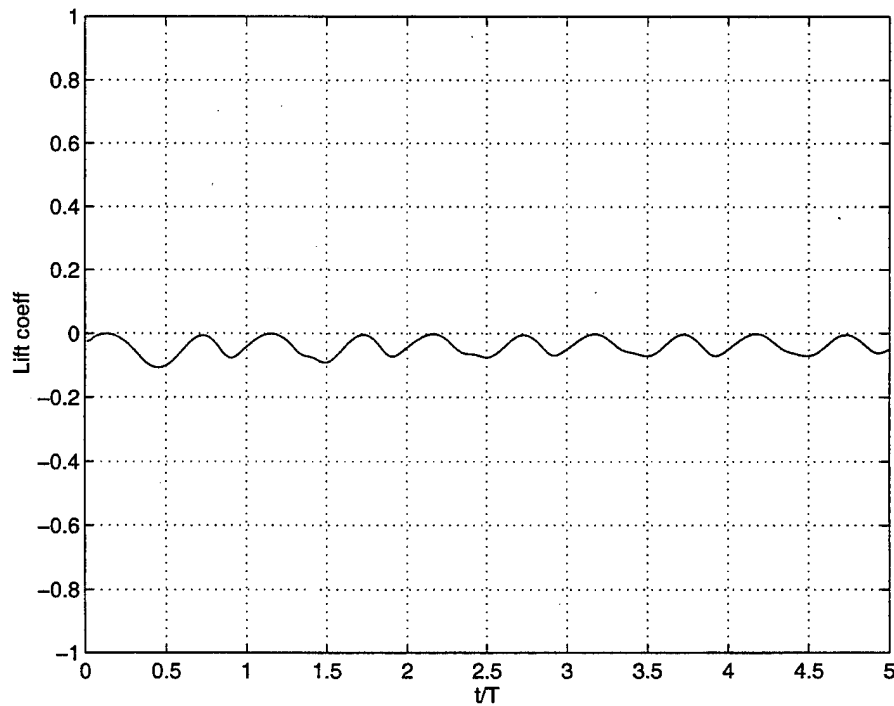


Figure 5b. Transverse force coefficient versus time.  $K=8.78$ ;  $\beta=1772$ ;  $V_k=4$

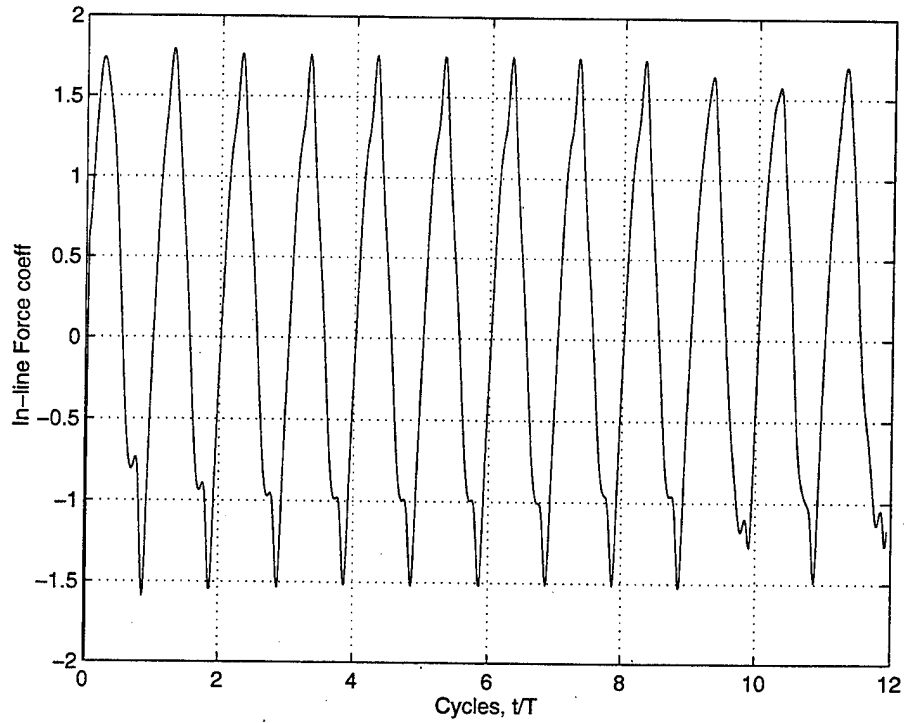


Figure 6a. In-line force coefficient versus time.  $K=12.19$ ;  $\beta=1772$ ;  $V_k=4$ . Inception of asymmetric vortex shedding at  $t/T \approx 7$ . (RNG turb. model)

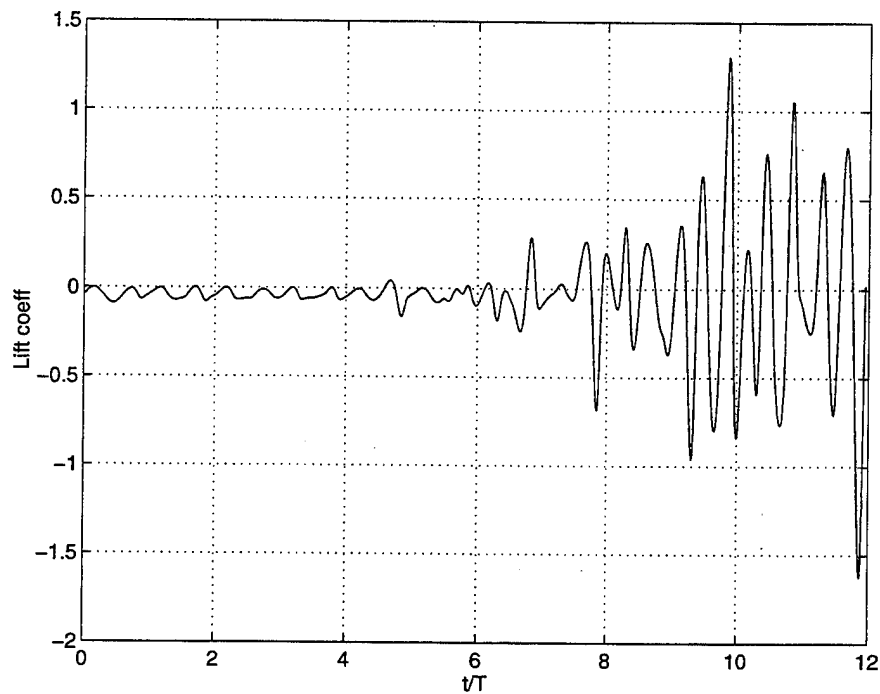


Figure 6b. Transverse force coefficient versus time.  $K=12.19$ ;  $\beta=1772$ ;  $V_k=4$ . Inception of asymmetric vortex shedding at  $t/T \approx 7$ . (RNG turb. model)

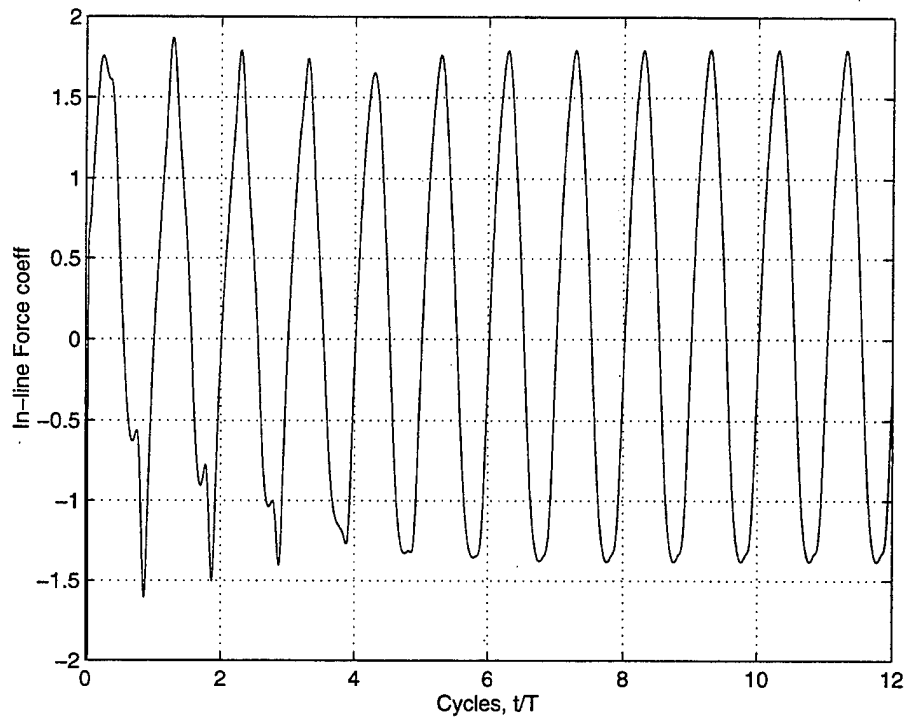


Figure 6c. In-line force coefficient versus time.  $K=12.19$ ;  $\beta=1772$ ;  $V_k=4$ . Inception of asymmetric vortex shedding at  $t/T \approx 3$ . (Low Re turb. model)

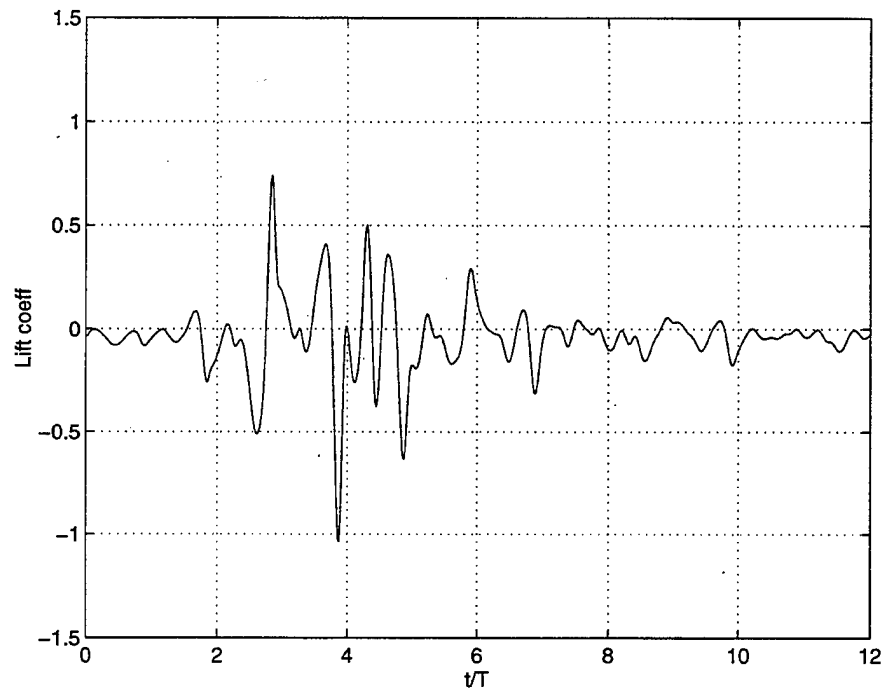


Figure 6d. Transverse force coefficient versus time.  $K=12.19$ ;  $\beta=1772$ ;  $V_k=4$ . Inception of asymmetric vortex shedding at  $t/T \approx 3$ . (Low Re turb. model)

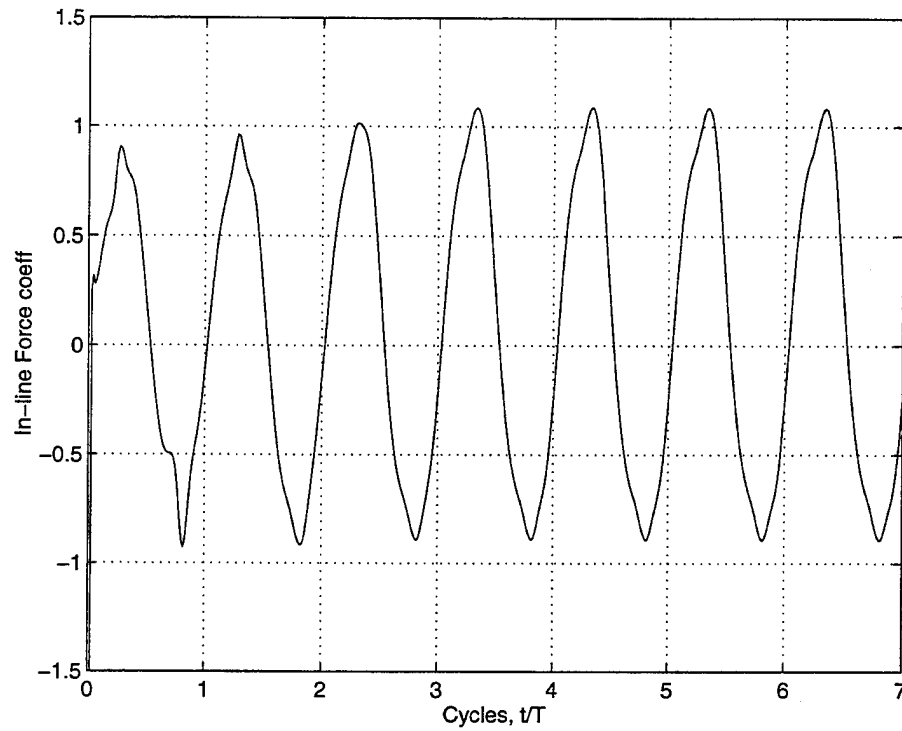


Figure 7. In-line force coefficient versus time.  $K=26.07$ ;  $\beta=1772$ ;  $V_k=4$

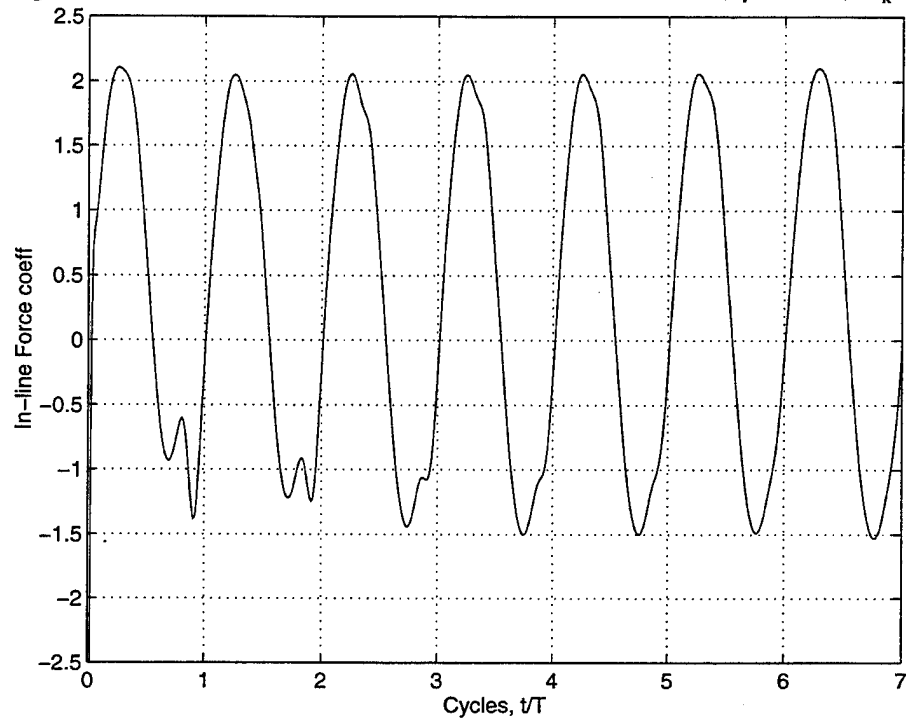


Figure 8. In-line force coefficient versus time.  $K=10.3$ ;  $\beta=1772$ ;  $V_k=6.05$   
Inception of asymmetric vortex shedding at  $t/T \approx 4$

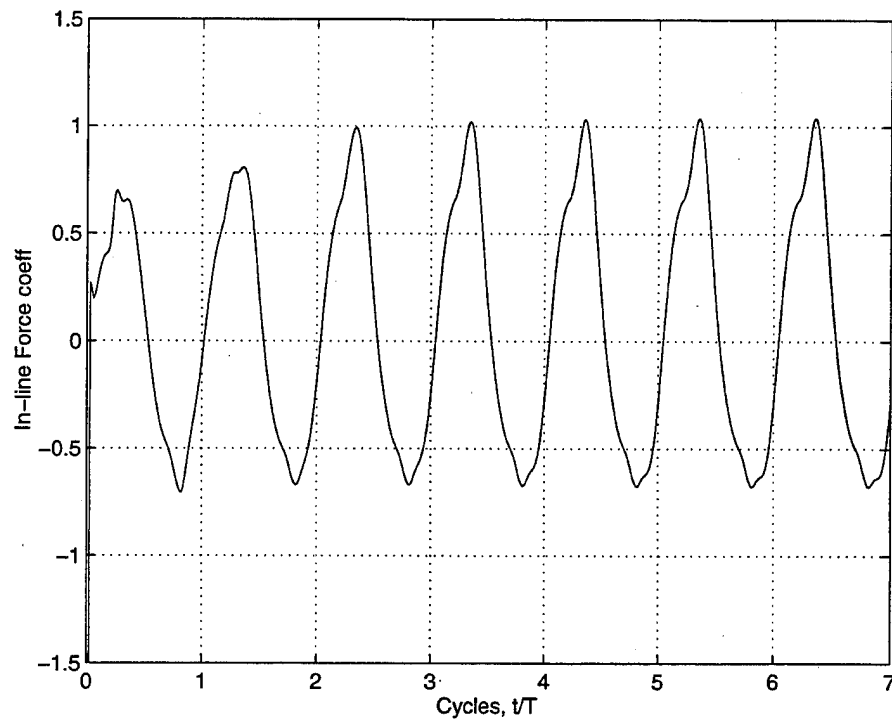


Figure 9a. In-line force coefficient versus time.  $K=36.5$ ;  $\beta=1772$ ;  $V_k=6.05$

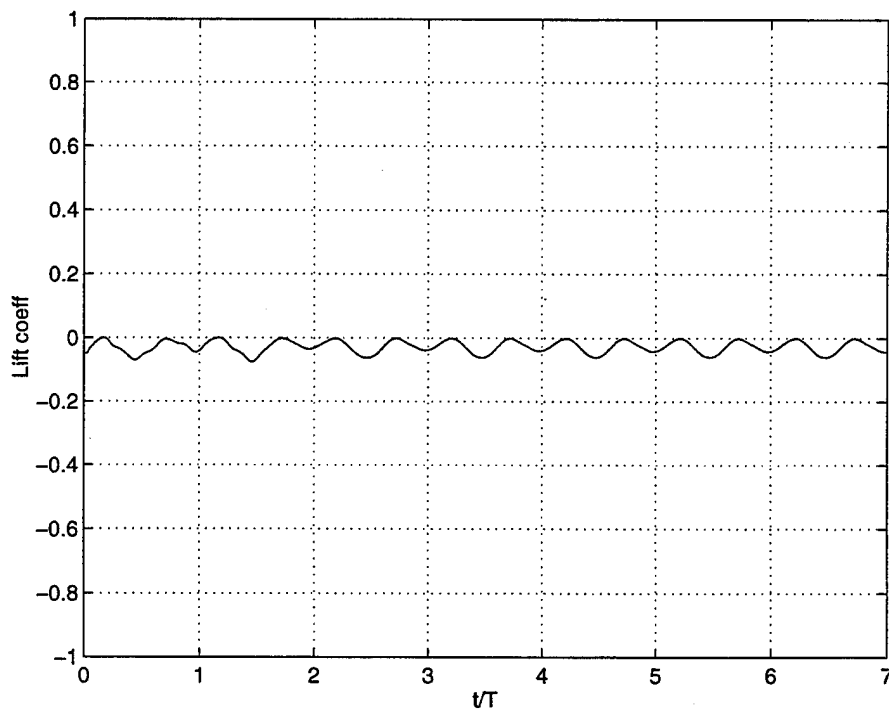


Figure 9b. Transverse force coefficient versus time.  $K=36.5$ ;  $\beta=1772$ ;  $V_k=6.05$

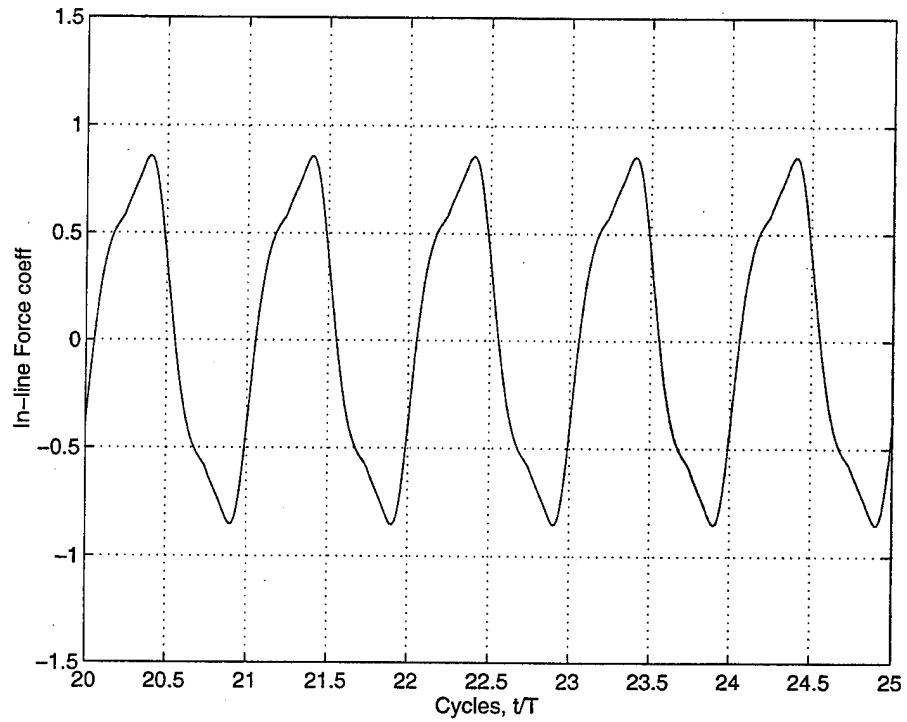


Figure 9c. In-line force coefficient versus time.  $K=36.5$ ;  $\beta=1772$ ;  $V_k=0$

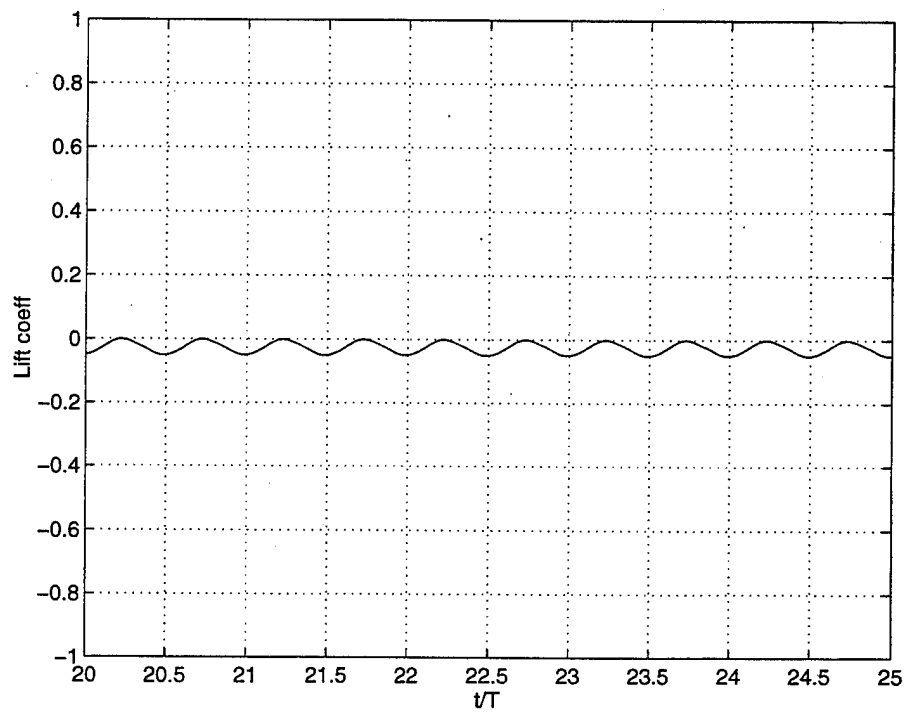


Figure 9d. Transverse force coefficient versus time.  $K=36.5$ ;  $\beta=1772$ ;  $V_k=0$

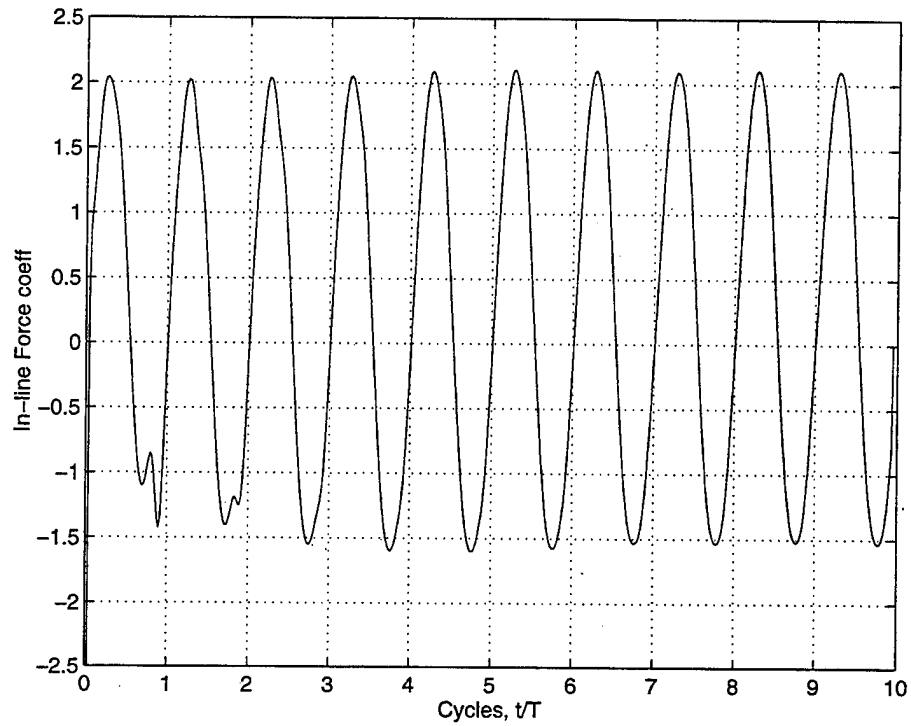


Figure 10. In-line force coefficient versus time.  $K=10.5$ ;  $\beta=2487$ ;  $V_k=5.01$   
Inception of asymmetric vortex shedding at  $t/T \approx 5$

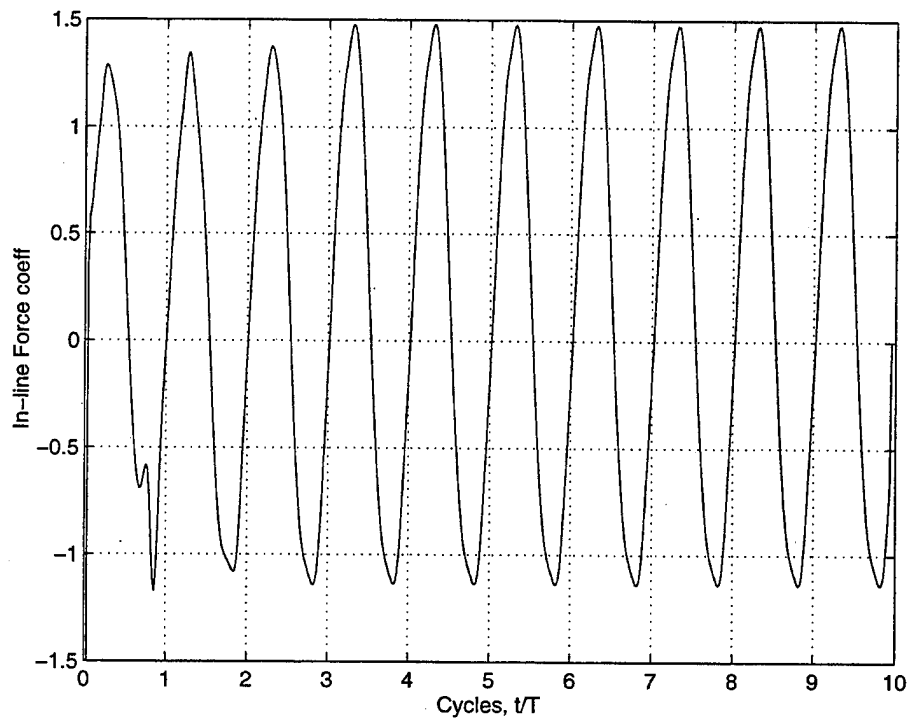


Figure 11. In-line force coefficient versus time.  $K=17.2$ ;  $\beta=2487$ ;  $V_k=5.01$

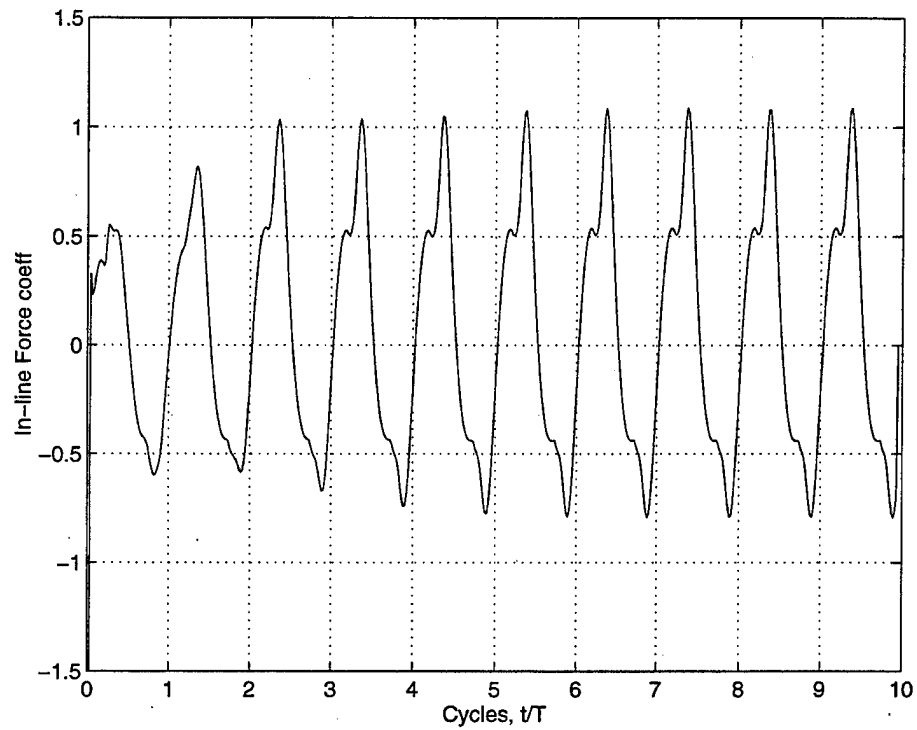


Figure 12. In-line force coefficient versus time.  $K=46$ ;  $\beta=2487$ ;  $V_k=5.01$

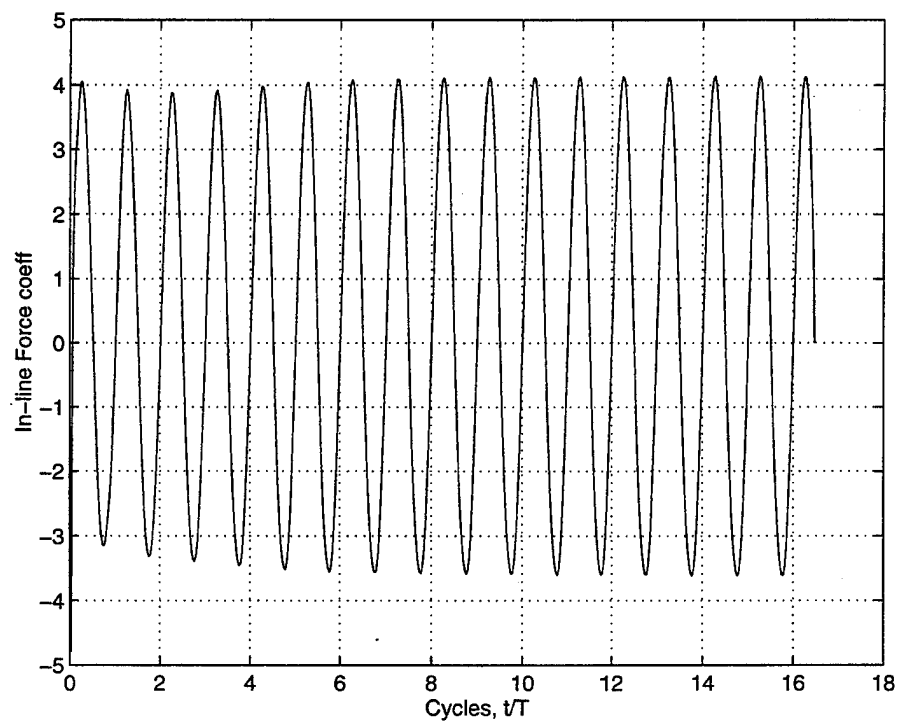


Figure 13. In-line force coefficient versus time.  $K=5.1$ ;  $\beta=4122$ ;  $V_k=2.07$

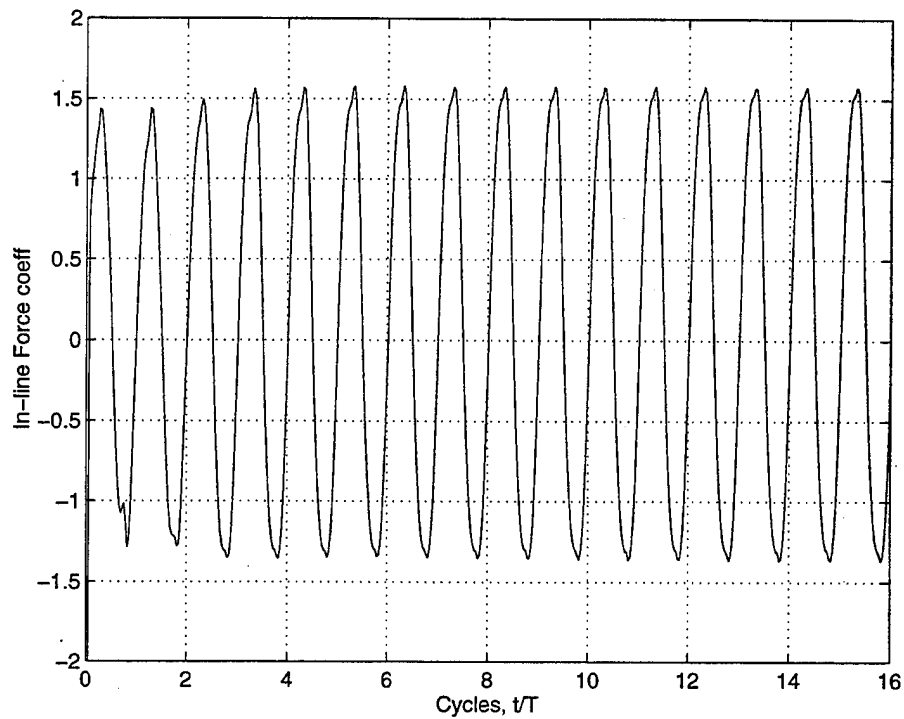


Figure 14a. In-line force coefficient versus time.  $K=15$ ;  $\beta=4122$ ;  $V_k=2.07$

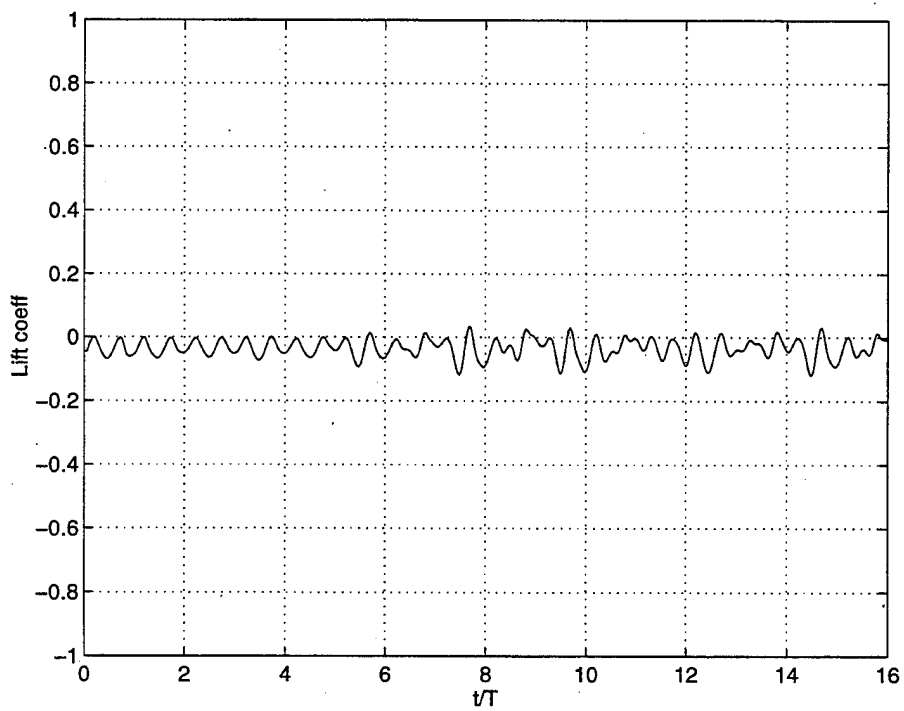


Figure 14b. Transverse force coefficient versus time.  $K=15$ ;  $\beta=4122$ ;  $V_k=2.07$

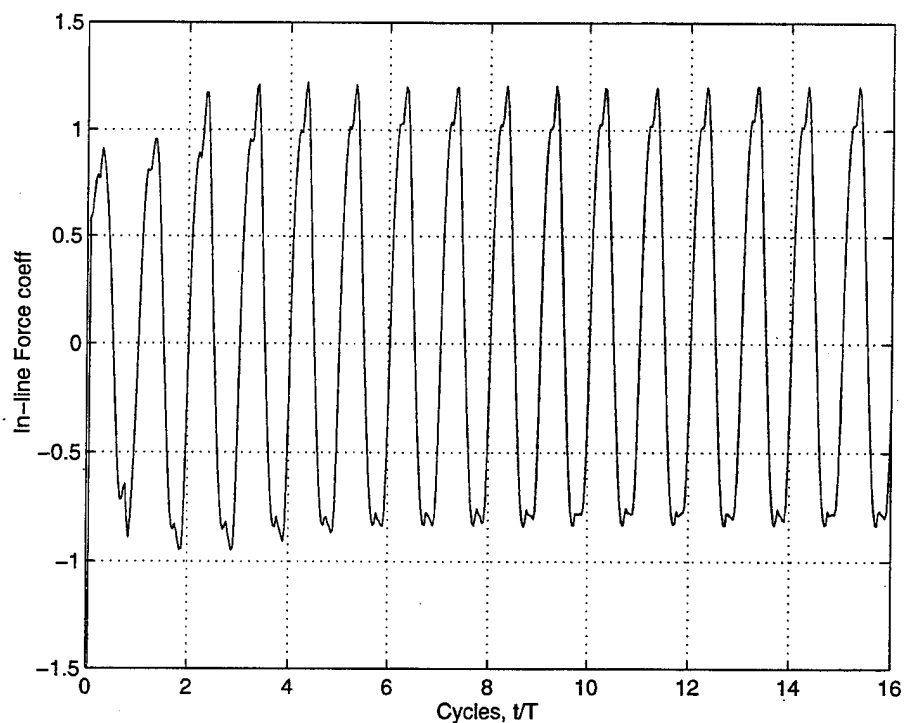


Figure 15a. In-line force coefficient versus time.  $K=24$ ;  $\beta=4122$ ;  $V_k=2.07$   
Inception of asymmetric vortex shedding at  $t/T \approx 4$

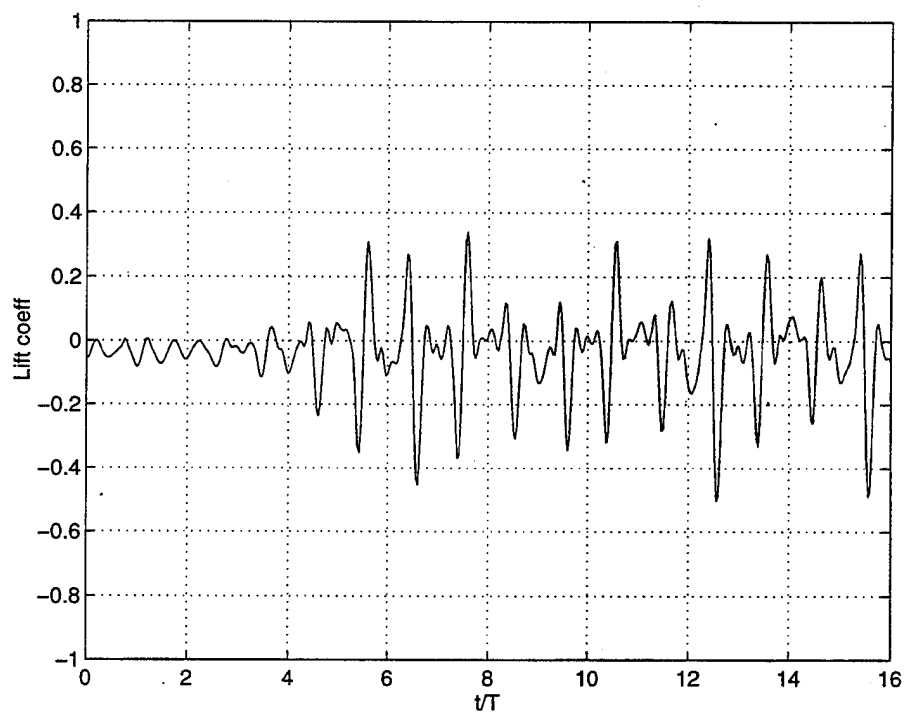


Figure 15b. Transverse force coefficient versus time.  $K=24$ ;  $\beta=4122$ ;  $V_k=2.07$   
Inception of asymmetric vortex shedding at  $t/T \approx 4$

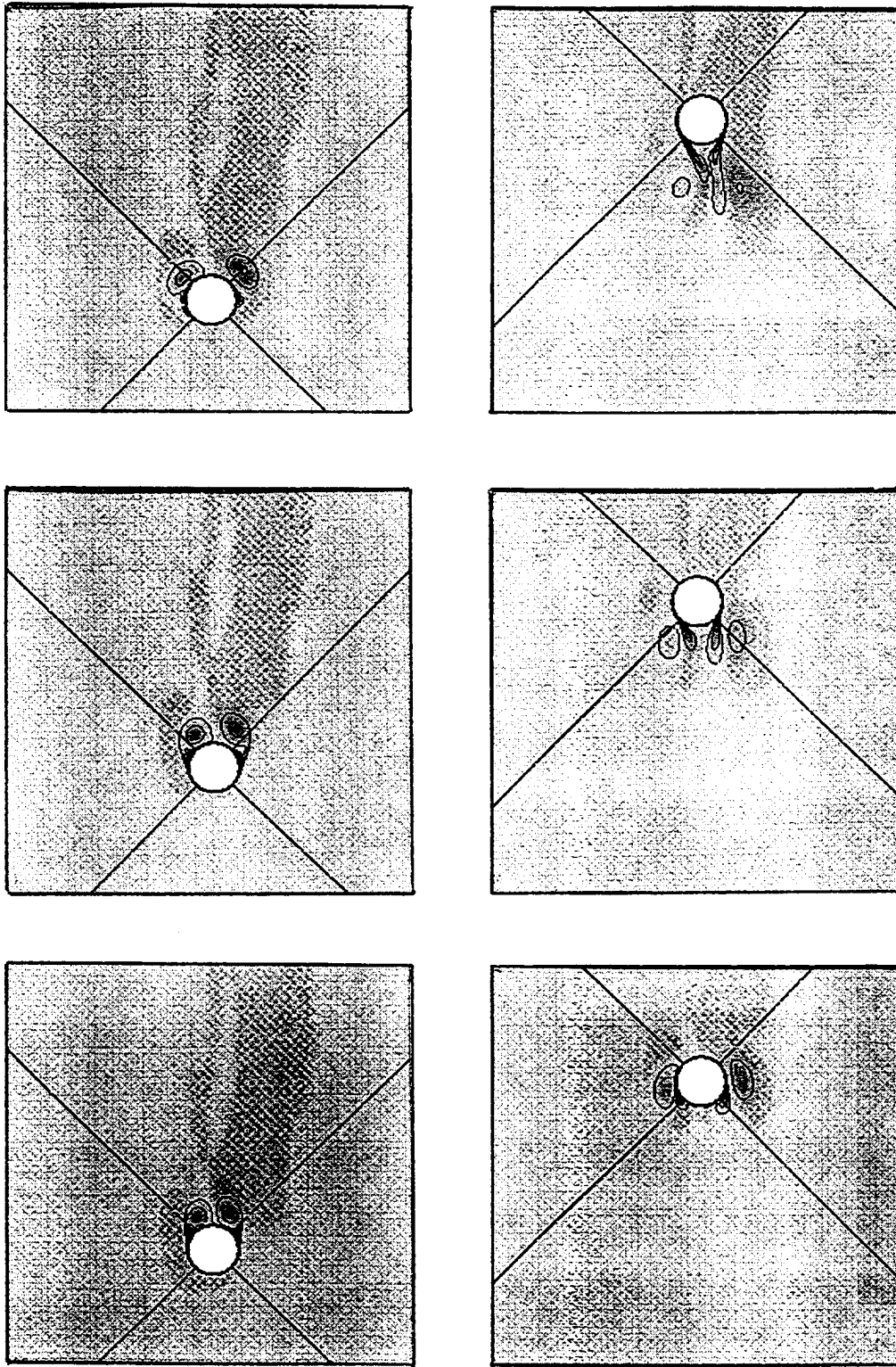


Figure 16. Evolution of vorticity.  $K=8.78$ ;  $\beta=1772$ ;  $V_t=0.43$ .  
a.  $U(t)/U_m = 0.99$ ; b.  $U(t)/U_m = 0.50$ ; c.  $U(t)/U_m = -0.02$ ; d.  $U(t)/U_m = -0.42$ ; e.  $U(t)/U_m = -0.58$ ; f.  $U(t)/U_m = -0.46$ .

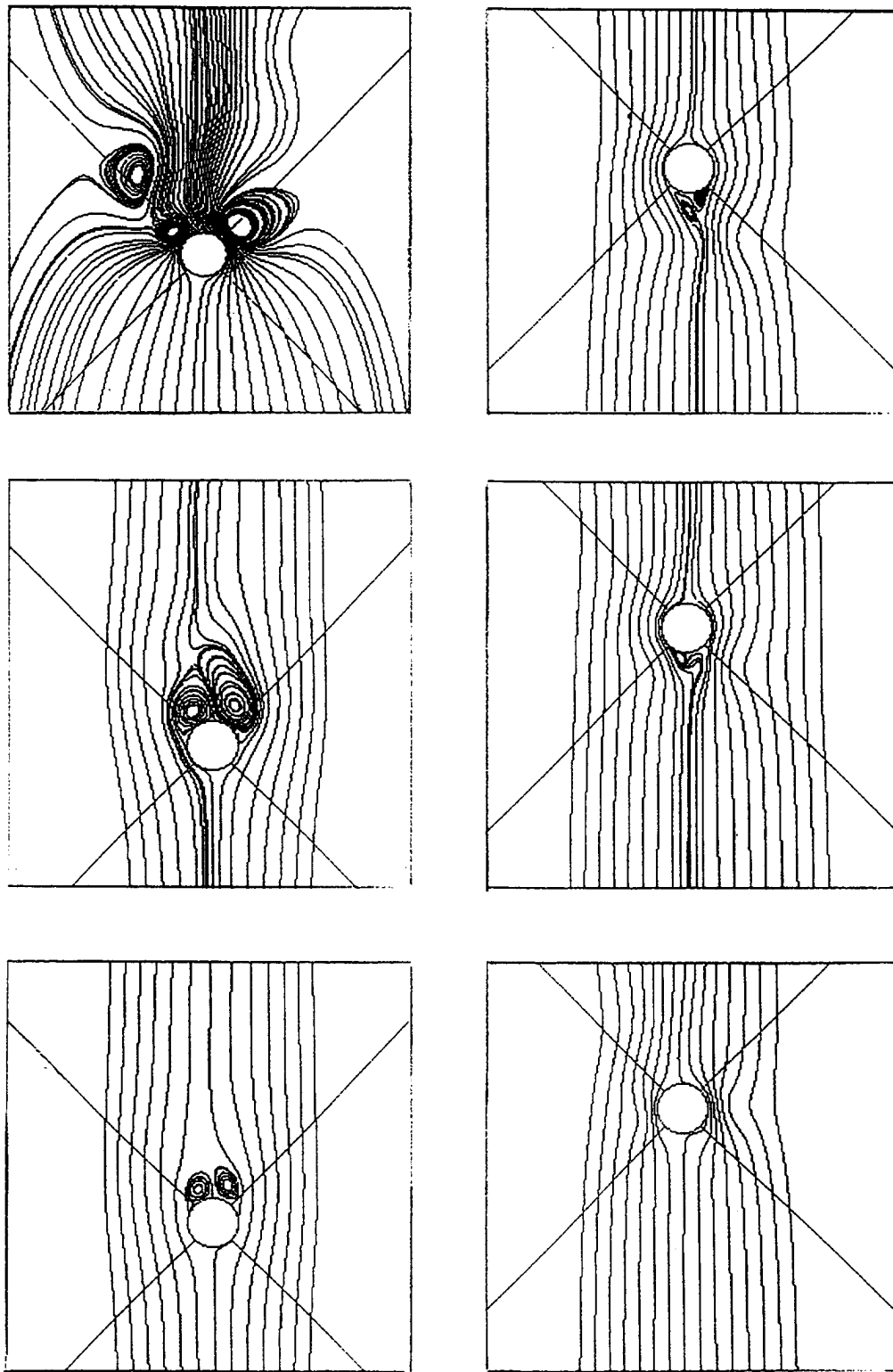


Figure 17. Streamlines.  $K=8.78$ ;  $\beta=1772$ ;  $V_r=0.43$   
a.  $U(t)/U_m = 0.99$ ; b.  $U(t)/U_m = 0.50$ ; c.  $U(t)/U_m = -0.02$ ; d.  $U(t)/U_m = -0.42$ ; e.  $U(t)/U_m = -0.58$ ; f.  $U(t)/U_m = -0.46$ .

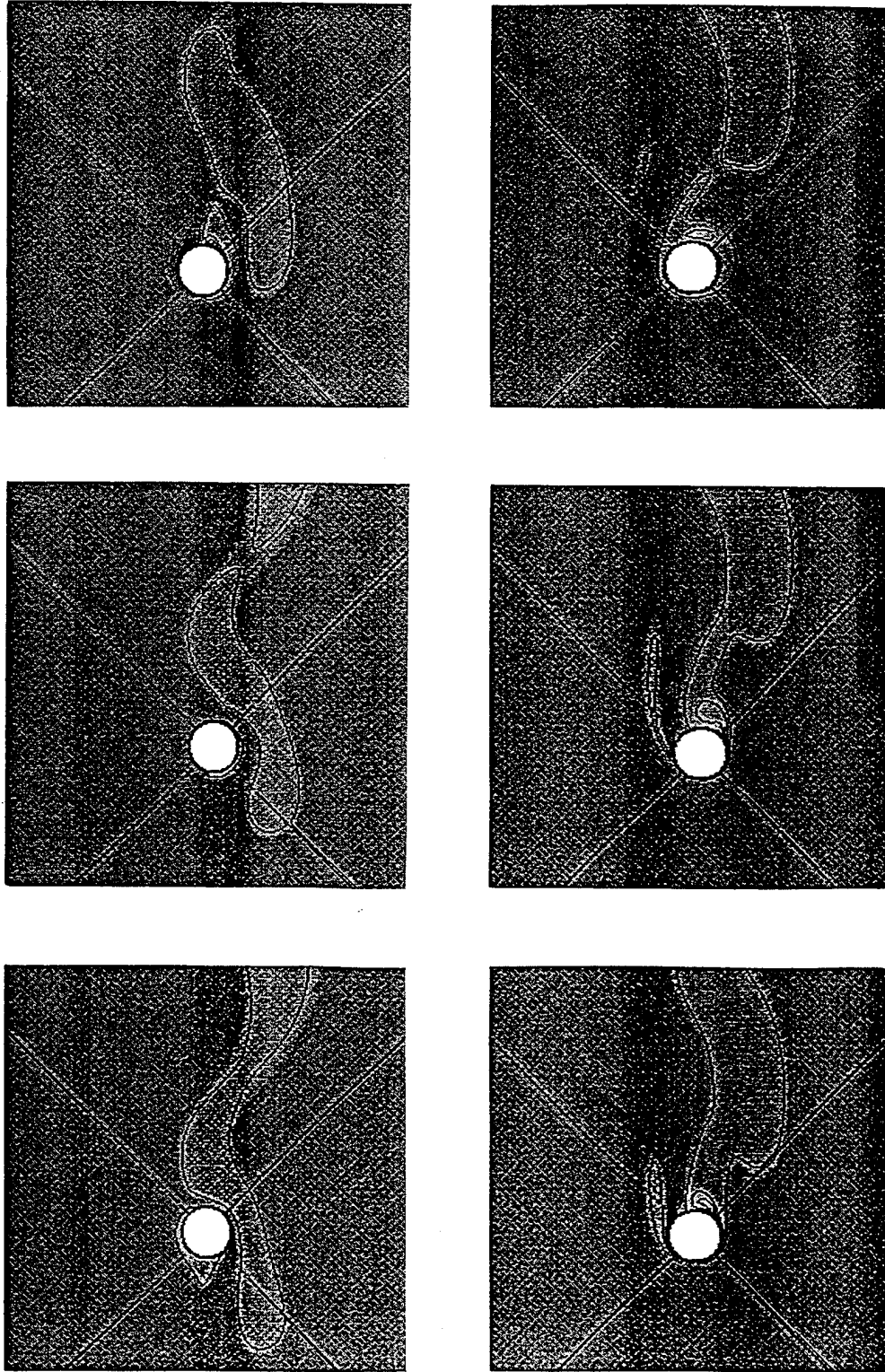


Figure 18. Evolution of vorticity.  $K=10.5$ ;  $\beta=2487$ ;  $V_r=0.47$

a.  $U(t)/U_m = 0.11$ ; b.  $U(t)/U_m = 0.98$ ; c.  $U(t)/U_m = 1.46$ ; d.  $U(t)/U_m = 1.22$ ; e.  $U(t)/U_m = 0.47$ ; f.  $U(t)/U_m = -0.29$ .

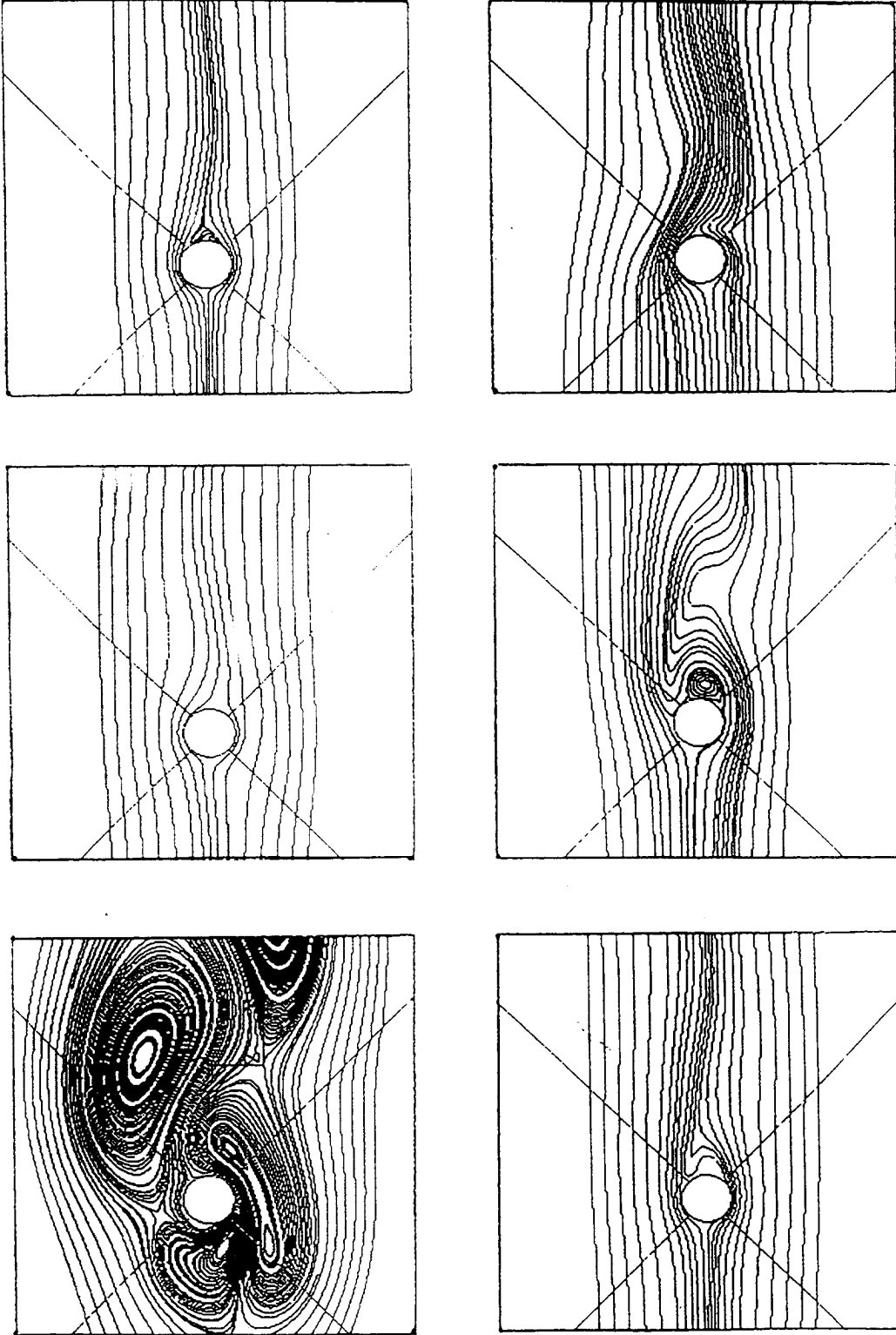


Figure 19. Streamlines.  $K=10.5$ ;  $\beta=2487$ ;  $V_r=0.47$   
a.  $U(t)/U_m = 0.11$ ; b.  $U(t)/U_m = 0.98$ ; c.  $U(t)/U_m = 1.46$ ; d.  $U(t)/U_m = 1.22$ ; e.  $U(t)/U_m = 0.47$ ; f.  $U(t)/U_m = -0.29$ .

## APPENDIX B.

### RECOMMENDED VALUES FOR THE CURRENT VELOCITY- PRESSURE DIFFERENTIAL CORRELATION COEFFICIENT

It was found experimentally that the coefficient  $C$  in equation [8] of section III D assumes different values as  $K$  and the computational time interval change. Since a considerable number of calculations were performed with a time interval of 0.02 seconds, the following table of recommended values for  $C$ , valid for time steps on the order of 0.02 seconds, is included. It should be realized that the recommended values constitute only a starting point and that further fine tuning might be necessary depending on how accurately the value of  $U_o$  is to be duplicated. One can infer from the table that, as  $K$  increases,  $C$  becomes closer to 0.5. In fact, when 0.5 was used in one steady flow case (which can be thought as a flow with an infinite value of  $K$ ), the correct value of ambient velocity was obtained.

As far as the dependence of  $C$  on the time interval, as a thumbrule  $C$  will assume values closer to 0.5 as the time interval is shortened. Unfortunately, the nature of this dependence has been noted only toward the end of this investigation so that not even an approximate quantitative definition of it can be formulated at this time.

Range of $K$ values	Recommended $C$ value
$<10$	0.5892
$10 \leq K < 18$	0.5721
$18 \leq K < 28$	0.5561
$28 \leq K < 38$	0.5411
$K \geq 38$	0.5261



## APPENDIX C. SAMPLE IN-FILE

TITLE 'K=36.5, Beta=1772, C1=158.49, Vk=6.05, T=1.41 coarse grid, no disturbance'

\*

\*

\*

\*

\*

\*\*\*\*\* Model \*\*\*\*\*

\*

\*

MODEL tcg115t

FUNCTIONS

PERIODIC WAVEPTOP C1=158.49 C2=2874.69 C3=4.453 C4=0 C5=0

PERIODIC WAVEPBOT C1=158.49 C2=2874.69 C3=4.453 C4=0 C5=0

PERIODIC WAVENTOP C1=-158.49 C2=-2874.69 C3=4.453 C4=0 C5=0

PERIODIC WAVENBOT C1=-158.49 C2=-2874.69 C3=4.453 C4=0 C5=0

END

\*

GEOMETRY

GRID 2D BFC

READ GRID FROM tcg.PFG

\* No Cell Types (Blockage or Solid) specified.

END

\*

PROBLEM\_TYPE

SOLVE FLOW TURBULENCE

UNSTEADY TF = 0 TL = 10 STEPS = 500

END

\*

## PROPERTIES

DENSITY CONSTANT 998

VISCOSITY CONSTANT\_KINEMATIC 1e-06

END

\*

## MODELS

TURBULENCE\_MODEL KE

END

\*

\*\*\* Boundary Conditions \*\*\*

\*

## BOUNDARY\_CONDITIONS

\* boundary condition: INTERFACE\_1\_1

INTERFACE 1 129 1 1 SOUTH

\* boundary condition: wall

WALL 1 1 1 64 WEST

U = 0 V = 0

\* boundary condition: outrighttop

EXIT\_P 129 129 32 64 EAST

U = 0 V = 0 P = FUNCTION\_WAVENTOP K = .000753 D = 0 L = 0.00225 T =

293

\* boundary condition: outrightbot

EXIT\_P 129 129 1 31 EAST

U = 0 V = 0 P = FUNCTION\_WAVENBOT K = .000753 D = 0 L = 0.00225 T =

293

\* boundary condition: INTERFACE\_1\_2

INTERFACE 1 129 64 64 NORTH

DOMAIN 2

- \* boundary condition: INTERFACE\_2\_1

INTERFACE 64 64 1 129 EAST

- \* boundary condition: wall

WALL 1 64 1 1 SOUTH

U = 0 V = 0

- \* boundary condition: symm

SYMMETRY 1 64 129 129 NORTH

- \* boundary condition: INTERFACE\_2\_2

INTERFACE 1 1 1 129 WEST

DOMAIN 3

- \* boundary condition: INTERFACE\_3\_1

INTERFACE 1 129 1 1 SOUTH

- \* boundary condition: outlefttop

EXIT\_P 1 1 32 64 WEST

U = 0 V = 0 P = FUNCTION\_WAVEPTOP K = .000753 D = 0 L = 0.00225 T =

293

- \* boundary condition: outleftbot

EXIT\_P 1 1 1 31 WEST

U = 0 V = 0 P = FUNCTION\_WAVEPBOT K = .000753 D = 0 L = 0.00225 T =

293

- \* boundary condition: wall

WALL 129 129 1 64 EAST

U = 0 V = 0

- \* boundary condition: INTERFACE\_3\_2

INTERFACE 1 129 64 64 NORTH

DOMAIN 4

- \* boundary condition: INTERFACE\_4\_1

INTERFACE 64 64 1 129 EAST

```

* boundary condition: symm
  SYMMETRY 1 64 1 1 SOUTH
* boundary condition: wall
  WALL 1 64 129 129 NORTH
  U = 0 V = 0
* boundary condition: INTERFACE_4_2
  INTERFACE 1 1 1 129 WEST
* No Momentum Resistances Defined
END
*
INITIAL_CONDITIONS
* Full field initial conditions
  U = -1.079 V = 0 P = 0 T = 293 K = .000753 D = 0 L = 0.00225
* RESTART FROM tcg43.2000.AUR
END
*
***** Solve *****
*
*
SOLUTION_CONTROL
  ALGORITHM SIMPLEC
  S_SCHEME UPWIND RHO K D
  S_SCHEME CENTRAL U V
  S_BLENDING 0.3 U V
  T_SCHEME EULER
  ITERATIONS 10
  C_ITERATIONS 1
  SOLVER WHOLE_I U V PP K D
  S_ITERATIONS 4 U V

```

S\_ITERATIONS 20 PP  
 S\_ITERATIONS 10 K D  
 INERTIAL\_FACTOR 0.2 U V  
 INERTIAL\_FACTOR 0.2 K D  
 RELAX 0.4 P  
 RELAX 1 RHO T VIS  
 MINVAL -1e+20 U V  
 MINVAL -1e+20 P  
 MINVAL 1e-06 RHO  
 MINVAL 1e-10 T VIS  
 MINVAL 1e-10 K D  
 MAXVAL 1e+20 U V  
 MAXVAL 1e+20 P RHO  
 MAXVAL 5000 T  
 MAXVAL 1e+20 VIS  
 MAXVAL 1e+20 K D  
 END  
 \*  
 OUTPUT  
 P\_FORCE ON PMIN = -1.e+05  
 PLOT3D ON FORMATTED  
 SCALAR\_FILE 1 RHO P T K STRM  
 DIAGNOSTICS OFF  
 MONITOR 2 32 129 U  
 MONITOR 4 32 1 U  
 TIME\_SAVE 250  
 UNIQUE\_NAME ON  
 END



## LIST OF REFERENCES

- Avva, R., Singhal, A., and Lai, Y., 1994, "Numerical Simulation of Periodic and 3-Dimensional Turbulent Flows with CFD-ACE," *ASME Fluids Engineering Division Summer Meeting*, Lake Tahoe, NV.
- Baba, N., and Miyata, H., 1987, "Higher-Order Accurate Difference Solutions of Vortex Generation from a Circular Cylinder in an Oscillatory Flow," *Journal of Computational Physics*, Vol. 69, pp. 362-369.
- CFD-ACE Theory Manual, 1993, CFD Research Corporation Huntsville, AL. 35805.
- Davis, R. W., and Moore, E. F., 1982, "A Numerical Study of Vortex Shedding from Rectangles," *Journal Fluid Mechanics*, Vol. 116, pp.475-506.
- Habchi, S., and Hufford, G., 1995, "Transient Simulation of Turbulent Flow Over Blunt Bodies," CFD Research corporation Huntsville, AL. 35805.
- Hanson, C. 1995, "Numerical Analysis of Oscillating Flow About a Circular Cylinder".
- Kato, M., and Launder, B. E., 1993, "The Modelling of Turbulent Flow around Stationary and Vibrating Square Cylinders," *9th Symposium on Turbulent Shear Flows*, Kyoto, Japan.
- Keulegan, G., and Carpenter, L., 1958, "Forces on Cylinders and Plates in an Oscillating Fluid," *Journal of Research of the National Bureau of Standards*, Vol. 60, No. 5, pp. 423-440.
- Murashige, S., Hinatsu, M., and Kinoshita, T., 1989, "Direct Calculations of the Navier-Stokes Equations for Forces Acting on a Cylinder in Oscillatory Flow," *Proceedings of the Eighth International Conference on Offshore Mechanics and Arctic Engineering*, The Hague, The Netherlands, Vol. 2, pp. 411-418.
- Rogers, S., 1994, "Progress in High-Lift Aerodynamic Calculations," *Journal of Aircraft*, Vol. 31, No. 6, pp. 1244-1251.
- Sarpkaya, T., 1976, "Vortex Shedding and Resistance in Harmonic Flow About Smooth and Rough Circular Cylinders at High Reynolds Numbers," Naval Postgraduate School Technical Report No. 59SL76021.
- Sarpkaya, T., Isaacson, M., *Mechanics of Wave Forces on Offshore Structures*, Van Nostrand Reinhold, New York City, 1981.

Sarpkaya, T., Putzig, C., Gordon, D., Wang, X., and Dalton, C., 1992, "Vortex Trajectories Around a Circular Cylinder in Oscillatory Plus Mean Flow," *Journal of Offshore Mechanics and Arctic Engineering*, Vol. 114 pp.291-298.

Storm, M., 1984, "Wave and Current Induced Forces on Cylinders," M.S. Thesis, Naval Postgraduate School, Monterey, CA.

# INITIAL DISTRIBUTION LIST

	No. Copies
1. Defense Technical Information Center 8725 John J. Kingman Rd. STE 0944 Ft. Belvoir, VA 22060-6218	2
2. Library, Code 13 Naval Postgraduate School Monterey, CA 93943-5101	2
3. Department Chairman, Code ME Department of Mechanical Engineering Naval Postgraduate School Monterey, CA 93943-5000	2
4. Professor T Sarpkaya, Code ME-S1 Department of Mechanical Engineering Naval Postgraduate School Monterey, CA 93943-5000	5
5. Curricular Officer, Code 34 Department of Naval/Mechanical Engineering Naval Postgraduate School Monterey, CA 93943-5100	1
6. LCDR Marc S. de Angelis 1518 Porter St. Philadelphia, PA 19145	1
7. Mrs. Concetta de Angelis Via G. B. Martini 2 Rome, IT 00198	1